NUCLEAR METHODS FOR SUBSEA FLUID CHARACTERIZATION

İlker Meriç

A dissertation submitted in partial fulfilment of the
requirements for the degree of Philosophiae Doctor (PhD) at
the Department of Physics and Technology
University of Bergen
Norway

April, 2012

PREFACE

This thesis is the result of a four year work on investigations regarding the use of nuclear measurement techniques for subsea fluid characterization. This thesis consists of a total of five papers, an introductory part with a detailed background and motivation of the current work as well as a presentation of the main results of the current work.

In 2003, research on the SOFA (Subsea Online Fluid Analyzer) concept was initiated by the Christian Michelsen Research AS in cooperation with the Department of Physics and Technology at the University of Bergen. The ultimate goal of the SOFA concept is to be able to characterize all of the components that may be found in a subsea hydrocarbon multiphase flow through utilizing multi-modality measurements. It also includes a module based on gamma-ray dual modality densitometry (DMD) for the characterization of produced water samples. The first part of the work presented in this thesis focuses on further improvements of the DMD measurement setup employed in the SOFA concept. This was done through experimental and Monte Carlo (MC) investigations of the feasibility of utilizing gas-filled Geiger-Müller (GM) counters for the detection of transmitted and scattered gamma-rays.

The DMD measurements alone are, however, not sufficiently sensitive to provide useful compositional information on produced water samples unless these are combined with other measurement modalities such as ultrasound and electrical conductivity measurements. The second part of the thesis, therefore, focuses on the experimental and MC work conducted in order to study the feasibility of applying the PGNAA (Prompt Gamma-ray Neutron Activation Analysis) method in conjunction with the MCLLS (Monte Carlo Library Least-Squares) approach for the characterization of produced water samples.

It would not have been possible to accomplish this work without very much appreciated help from people who have shown a great deal of interest, and provided a great deal of help. First of all, I would like to thank my supervisors Prof. Geir Anton Johansen (University of Bergen, Norway), Dr. Marie Bueie Holstad (Christian Michelsen Research AS, Norway) and Prof. Robin Pierce Gardner (North Carolina State University, USA) for fruitful discussions and much appreciated feedback. Also, I would like to thank the staff at the mechanical workshop at Department of Physics and Technology at the University of Bergen as well as the staff at the precision instrument machine shop at the North Carolina State University for the good co-operation. The members of the Center for Engineering Applications of Radioisotopes (CEAR) as well as the staff at the Department of Nuclear Engineering at the North Carolina State University deserve a special thank you for their extremely welcoming attitude and willingness to co-operate during my six months visit (October 2010 – April 2011). I also would like to thank Dr. Rachid Maad for his help during my laboratory work at the Department of Physics and Technology, Dr. Silvio de Barros Melo for useful discussions on mathematics as well as Dr. Ketil Røed for proof-reading this manuscript and providing useful feedback regarding its contents.

Last but not least, I would like to thank my family and friends for their support during last four years. A special thank you goes to my wife, Iva Srot, for being there for me and providing a great deal of support whenever needed.

Bergen, 20 April 2012

İlker Meriç

Table of Contents

Paper 1: *Monte Carlo modelling of gamma-ray stopping efficiencies of Geiger-Müller counters,*
I. Meric, G. A. Johansen, M. B. Holstad, R. P. Gardner
Nuclear Instruments and Methods in Physics Research A **636** (2011) 61-66

Paper 2: *A single scatter electron Monte Carlo approach for simulating gamma-ray stopping efficiencies of Geiger-Müller counters,*
I. Meric, G. A. Johansen, M. B. Holstad, K. O. Lee, A. F. Calderon, J. Wang, R.P. Gardner
Nuclear Instruments and Methods in Physics Research A **654** (2011) 279-287

Paper 3: *Produced water characterization by prompt gamma-ray neutron activation analysis,*
I. Meric, G. A. Johansen, M. B. Holstad, J. Wang, R. P. Gardner
Measurement Science and Technology **22** (2011) 125701

Paper 4: *On the treatment of ill-conditioned cases in the Monte Carlo library least-squares approach for inverse radiation analyzers,*
I. Meric, G. A. Johansen, M. B. Holstad, J. Mattingly, R. P. Gardner
Measurement Science and Technology **23** (2012) 055603

Paper 5: *Enhancement of the intrinsic gamma-ray stopping efficiency of Geiger-Müller counters,*
I. Meric, G. A. Johansen, M. B. Holstad, A. F. Calderon, R. P. Gardner
Submitted to Nuclear Instruments and Methods in Physics Research A

1. Introduction

In this chapter, an introduction to this thesis will be given. First of all, a background of the current work will be presented. Then, a section will be dedicated to the relevant previous work and the motivation for carrying out the current projects. Moreover, projects included in this work will be briefly introduced. Finally, as the main computational tool in this work is the Monte Carlo (MC) radiation transport simulation, a very brief introduction to the MC method will be provided.

1.1 Background

The focus of this work has been to evaluate the use of nuclear measurement systems for subsea fluid characterization. In spite of environmental concerns, nuclear measurements have been and still are utilized in several different contexts within the industry. This is because industrial gauges based on measurements of radiation offer a rapid, on-line, non-intrusive and non-destructive way of analyzing numerous samples of interest. Typical examples are the gamma-ray densitometers which are frequently employed within e.g., mining and metallurgical industries, food and animal feed processing and within the petroleum industry for void fraction, i.e. the gas volume fraction, measurements [1-4]. Also, the application of measurements of neutron induced prompt gamma-rays, i.e. the prompt gamma-ray neutron activation analysis (PGNAA) method, was recently evaluated for multiphase flow measurements [5]. Furthermore, recent feasibility studies with nuclear gauges based on measurements of transmitted and scattered gamma-rays, i.e. the so-called gamma-ray dual modality densitometry (DMD) principle, have been conducted in conjunction with scintillation detectors to perform salinity independent measurements of void fraction in an offshore multiphase flow [6, 7]. In addition, gauges based on measurements of gamma-rays and neutrons have been used for oil well-logging applications [8, 9]. Naturally, all of these measurement systems mentioned here have their pros and cons. However, addressing the issues related to all of these would be out of the scope of this work. Therefore, this work focuses on the potential use of the PGNAA method in connection with offshore fluid characterization as well as on the use of alternative ionizing radiation detectors that could be employed in the gamma-ray DMD measurement principle.

In the petroleum industry, the general trend is to abandon the use of traditional topside production facilities and instead, focus on potential production and processing facilities at the seabed. Accordingly, there is an even greater demand on more accurate, prompt and non-intrusive multiphase gas/oil/water measurement systems that require minimal maintenance and that, preferably, exhibit stable operation under more demanding conditions.

As a response to the increasing demands for subsea instrumentation within the offshore oil and gas industry, Christian Michelsen Research (CMR) AS has initiated the SOFA (Subsea On-line Multiphase Fluid Sampling and Analysis System) concept in cooperation with the Department of Physics and Technology at University of Bergen (UoB). The SOFA project was initiated in 2003. Several feasibility studies were carried out to determine the optimal system parameters, and these studies are still ongoing. The main purpose of the SOFA concept is to allow characterization and monitoring of all of the individual components that may be found in a multiphase flow in connection with the offshore hydrocarbon production. An example use of the SOFA concept may be as a permanently installed subsea autonomous metering station so that transportation of fluid samples to the surface by remotely operated vehicles (ROVs) can be avoided. This would then lead to a significant reduction in the

operational costs keeping in mind that the traditional multiphase flow meters that are frequently employed in topside and subsea hydrocarbon production facilities require input parameters such as oil permittivity and gas density for proper operation. A schematic of the SOFA concept as well as that of a traditional multiphase flow meter are given in figure 1.1.

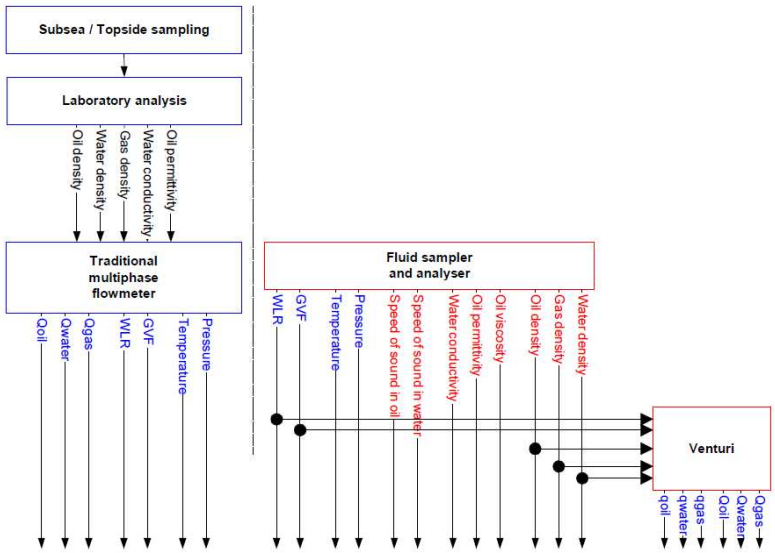

Figure 1.1 Schematic of the SOFA concept is given on the right-hand side. Also given is the schematic of a traditional multiphase flow meter (on the left-hand side) for comparison purposes. In this figure, q is the volumetric flow rate of the components, Q is the mass flow rate of the components, WLR is the volumetric water to liquid ratio and GVF is the gas volume fraction [10, 11].

As can be seen in figure 1.1, the SOFA system can be used in conjunction with a traditional venturimeter in cases where the volumetric and mass flow rates of the individual components are required. Also, it is clear from figure 1.1 that the SOFA system will eliminate the need for laboratory analyses of fluid samples carried out to determine critical parameters needed to maintain proper operation of traditional multiphase flowmeters and is therefore expected to be a cost efficient means for optimization of subsea separation processes and well management.

The SOFA concept will be designed to take advantage of a number of different modules and technologies in order to perform all of the required measurements. Once the individual fluid properties are determined, these may then be utilized to further improve multiphase flow meter readings and to optimize hydrocarbon processing, well management and production allocation. Previously, an experimental prototype of the SOFA measurement system was built by CMR AS and UoB (see figure 1.2 and figure 1.3). There are two major challenges in conjunction with the development of the SOFA concept. The first one is, as pointed out in [10, 11], taking representative samples from the process line. The second important challenge is performing as accurate and prompt measurements as possible on the individual multiphase components. The challenges associated with the former, i.e. the representative sampling problem, are not treated in this work. Nevertheless, the interested reader is referred to [10-12] for a thorough discussion of the subject.

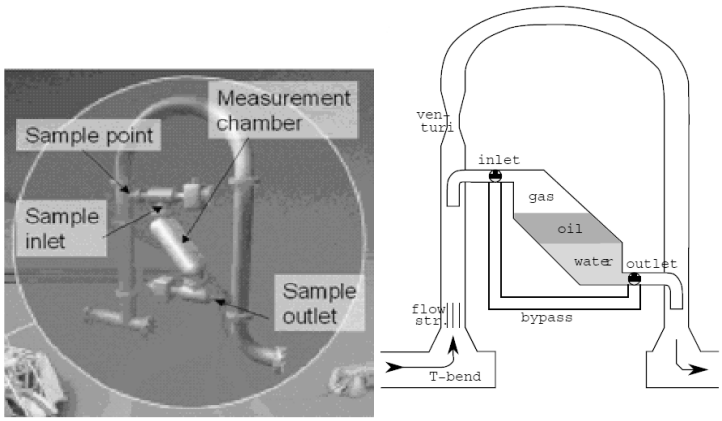

Figure 1.2 An illustration of the prototype of the SOFA concept built by CMR and UoB (to the left). Samples are taken from the process line through a pitot tube (to the right). The multiphase fluid sample is then transferred into the measurement chamber where the pertinent measurements take place to characterize the components in a deep sea multiphase flow [10, 13][1].

As can be seen in figure 1.2, the experimental prototype of the SOFA concept consists of a measurement chamber where relevant measurements take place to characterize the components in a deep sea multiphase flow. A sample from the multiphase flow is taken through a pitot tube introduced into the main process line. A more detailed description of the concept can be found in [10-12]. As soon as the fluid sample is transferred into the measurement chamber, both inlet and outlet valves are closed. Then, the individual phases are left to separate prior to performing measurements. Several measurement modalities will be employed in order to enable the characterization of all of the individual components. As an example; ultrasonic measurements are performed to determine the phase levels within the chamber and the volume fractions of each of the components.

Among others, the SOFA concept will also be utilized to characterize produced water samples. Throughout the work presented in this thesis, the focus is on the challenges associated with the characterization of produced water samples. Detailed characterization of produced water samples implies determination of salinity and preferably, a compositional analysis of various produced water samples. Formation water can be defined as the water that is found in the reservoirs prior to hydrocarbon production. On the other hand, produced water is the water phase that is produced together with oil and gas phases during hydrocarbon recovery. This should not be confused with formation water as produced water is usually a mixture of formation water and the injected seawater. Characterization of produced water samples is a crucial part of the subsea process and production optimization and monitoring. This is because the composition of produced water may vary as a result of the location and throughout the lifetime of a field [14] as well as relatively sudden changes in the produced water salinity (the weight fraction of salt in water) and composition, such as when the injected seawater breaks through to another production well, may reveal critical changes in the production conditions (see table 1.1). Formation water and seawater typically contain different amounts and types of salt ions, and the typical salt ion concentrations that can be found in seawater and formation water are presented in table 1.1.

[1] The figure on the left-hand side is reproduced with permission from the publisher (IOP Publishing Ltd.).

Table 1.1 **Typical salt ions found in formation water and seawater. As can be seen, formation water and seawater typically have different chemical compositions [13].**

Ions	Formation water [mg/l]	Seawater [mg/l]
Sodium Na^+	30730	10500
Potassium K^+	710	390
Magnesium, Mg^{2+}	470	1350
Chlorine Cl^-	59640	19000
Calcium Ca^{2+}	5300	410
Barium Ba^{2+}	420	<1
Strontium Sr^{2+}	840	8
Sulphate SO_4^-	4	2700

Another important issue is that, in the petroleum industry, many other measurements, for instance electrical impedance measurements, show a great dependence on the salinity of the water phase [13, 15]. These measurements would need to be compensated for possible changes in the water salinity. Accurate measurements of salinity of the water phase will also be critical in determining the individual flow rates of gas, oil and water in the process line [16]. Thus, the ability to carry out accurate measurements of the water salinity is of significant importance.

1.2 Previous work and motivation

Previously, the feasibility of using the so-called gamma-ray DMD principle for the characterization of produced water samples was investigated through experiments and MC simulations [13, 17]. The DMD principle is, as mentioned earlier, based on measurements of gamma-rays transmitted and scattered in the sample of interest.

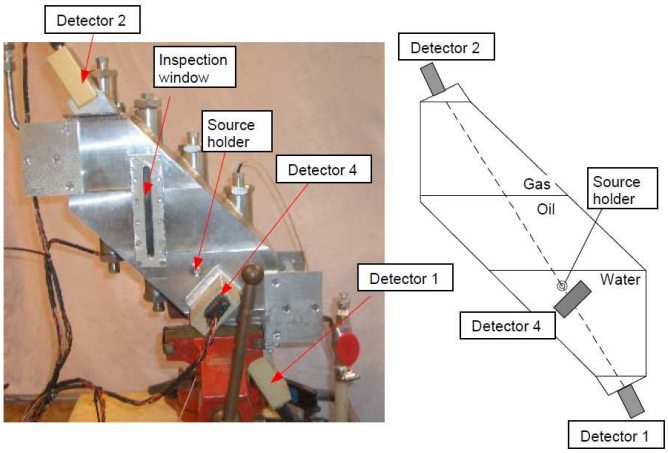

Figure 1.3 **A cross-sectional view of the SOFA measurement chamber. The 100 mCi ^{241}Am source with emission energy of 59.5 keV, is placed inside the measurement chamber. This will allow avoiding unnecessary attenuation of gamma-rays within the chamber walls as well as allowing direct transmission measurements through all three phases, i.e. gas, oil and water. Detector 3 is placed at the opposite side of the source in order to measure transmitted gamma-ray intensity [11].**

The measurement chamber was, therefore, designed to accommodate the gamma-ray detectors as well as the radioisotopic gamma-ray source required to perform these measurements. A cross-sectional view of the measurement chamber showing the locations of the radioisotopic source, i.e. the 100.0 mCi ^{241}Am source with principal emission energy of 59.5 keV, and the detectors is provided in figure 1.3. As can be seen in figure 1.3, the source is mounted using a screw-like, thin-walled stainless steel source holder. This allows the source to be placed within the measurement chamber, in direct contact with the fluid sample, and thus, avoids undesired attenuation of the primary gamma-rays in the chamber walls.

In the SOFA prototype, a total of four semiconductor detectors were installed in order to study the feasibility of the DMD approach for measurements on the produced water samples. Detectors 1, 2 and 3 were used for transmission measurements whereas detector 4 was used for the measurements of scattered gamma-rays. In order to achieve good counting statistics within short integration times (about 2 min. [10]), CdZnTe semiconductor detectors were used in the measurements as well as in the subsequent MC calculations [10, 11, 13, 17]. It should, however, be pointed out that only detectors 1, 3 and 4 were utilized for measurements on the water phase. Detectors 1 and 3 were used to measure the intensity of the transmitted gamma-rays through the water phase whereas detector 4 was used to measure the intensity of the scattered gamma-rays from the water component.

The basic idea behind the implementation of the DMD principle for the characterization of the produced water samples has been to perform both transmission and scatter measurements simultaneously in order to be able to extract as much information as possible from the sample under investigation. It was thought that this would be enabled by the fact that transmission measurements will depend strongly on the effective atomic number of the sample as the photoelectric absorption cross-section is proportional to Z^{4-5}. This would mean that the transmission measurements would be highly sensitive to the salt content of produced water samples. The scatter measurements, on the other hand, will depend essentially on the density of the fluid sample. Thus, the transmission and scatter measurement results will provide independent measurement results. This also explains the choice of radioisotope in this case, i.e. the ^{241}Am source, since at energy of 59.5 keV both photoelectric effect and Compton scattering will have about the same contribution to the total attenuation of photons in the materials of interest [1].

It was seen that the preliminary experimental feasibility measurements with the measurement geometry shown in figure 1.3 and the results of MC simulations confirm the above observation. Details of these calculations can be found in [10, 11, 13, 17]. In conclusion, it was seen that the DMD principle would be highly sensitive to the overall salt content in brine, i.e. the salinity, and would therefore, be feasible for accurate calculations of salinity.

The motivation for pursuing the work presented in this thesis has been two important properties related to the DMD principle employed in the prototype of the SOFA concept. These properties can be listed as follows:

- The fact that the preliminary measurements and MC simulations with the DMD measurement setup were carried out using CdZnTe detectors mainly because these detectors can essentially detect all incident 59.5 keV gamma-rays, i.e. they have essentially 100% stopping efficiency at this energy. Nonetheless, in a potential field application of the DMD measurement principle, gas-filled ionizing radiation

detectors, such as Geiger-Müller (GM) counters could prove to be much more suitable, mainly due to their robustness in harsh environments and low costs compared to semiconductor detectors.

- In many cases, the ability of the DMD principle to perform accurate measurements of the salinity will be sufficient. However, the monitoring of transmitted and scattered gamma-rays alone will not be sufficiently sensitive in cases where there is specific need for more information on the produced water samples, such as the identification of salt ions that may be present in the pertinent produced water samples. It has been pointed out that only a combination of gamma-ray transmission and scatter measurements, permittivity measurements and ultrasound measurements would provide useful information on the composition of produced water samples [10].

Of the two facts mentioned above, the latter represents a serious limitation in the application of the DMD principle in connection with the characterization of produced water samples. In this thesis, this limitation of the DMD principle will be addressed through the use of an alternative radioisotope gauge based on the PGNAA method. The PGNAA method is briefly introduced in the following section. Addressing the former fact, on the other hand, represents a possible improvement of the DMD principle in case it is to be considered in the final design of the SOFA concept. Possible utilization of GM counters in the DMD measurement setup would bring with it certain advantages as well as disadvantages. These are also briefly discussed in the following section.

1.3 Projects included in this thesis

This thesis includes two separate projects both of which are related to the subsea characterization of produced water samples. The first project is related to the DMD principle which has already been considered for this purpose. In the first part of the work presented in this thesis, the focus is on further improvements of the DMD measurement setup through investigations of the applicability of GM counters in the DMD setup. The second part, on the other hand, is focused on investigations regarding the feasibility of applying the PGNAA method for the characterization of produced water samples as an alternative to the gamma-ray DMD measurement principle.

As mentioned in the previous section, the feasibility studies with the DMD principle were carried out using CdZnTe semiconductor detectors as these detectors exhibit essentially 100% gamma-ray stopping efficiency at the energy of interest, i.e. 59.5 keV. Utilization of CdZnTe semiconductor detectors in the DMD principle could be realized in spite of their sensitivity to temperature changes and mechanical vibrations. This is related to the fact that the temperature at the seabed will be stable at about 4ºC as well as the fact that the effects of mechanical vibrations could be minimized by placing the detectors in silicon beds [1] which, in turn, help maintaining stable operation. On the other hand, in case the DMD principle is to be pursued in the final design of the SOFA concept, the entire measurement system could be made to be more robust and cost-effective by utilizing gas-filled GM counters instead of CdZnTe detectors. This is because GM counters are known to be versatile, robust, and insensitive to temperature and pressure changes as well as mechanical vibrations. These properties of GM counters, together with the fact that they require relatively simple read-out electronics and their relatively low costs, make them a popular choice in applications that do not require energy sensitivity. Therefore, these counters have found many applications within the

industry especially if measurements are to be performed in harsh environments such as in the Tracerco Profiler™, which is a multiple source/detector system for measurement of component phase heights in gas/oil/water gravity separators [1]. In addition, due to extremely high temperatures, stable operation may not be maintained using CdZnTe semiconductor detectors in case a similar instrument based on measurements of transmitted and scattered gamma-rays is to be utilized in downhole measurements. Therefore, there has been an increasing interest in the use of GM counters in the DMD measurement setup described above [2, 18]. However, there is a serious downside to the use of GM counters in such applications, especially if short integration times are required. As these are gaseous detectors, their intrinsic gamma-ray stopping efficiencies will be relatively poor, approximately about 1.0% over a wide range of photon energies [1, 2, 19, 20]. This detection efficiency is much less than what can be achieved using solid state detectors such as CdZnTe semiconductor and NaI(Tl) scintillation detectors [1]. For a given integration time and a given source activity, the poor gamma-ray detection efficiencies of GM counters may lead to very low signal-to-noise ratio (SNR) values in the measurement results with respect to other, more efficient solid state detectors. Also, it could be necessary to consider increasing the source strength accordingly in order to achieve better SNR values. According to the ALARA (As Low As Reasonably Achievable) principle [1], this could make the use of GM counters in such cases unjustifiable. Therefore, the first project in this thesis focuses on the identification of a method whereby the relatively poor gamma-ray intrinsic stopping efficiency[2] of these detectors could be improved. The approach taken is to first develop benchmarked MC models and thereafter utilize these MC models to investigate certain geometric modifications of the GM counter that could increase its sensitivity to incident low energy (59.5 keV) gamma-rays. A more detailed discussion on this issue is given in chapter 2. The results of this project are presented in detail in a series of papers (see papers 1,2 and 5). A brief presentation of the main results relevant to this project can also be found in chapter 2.

As mentioned in the previous section, the DMD measurements alone are not sufficient to provide detailed information on the chemical composition of produced water samples. Such information can only be achieved if several measurement modalities are utilized simultaneously.

A well-known elemental analysis technique is the PGNAA method which found many applications within the industry such as analysis of food, coal and oil well-logging [9, 21-24]. The PGNAA method is based on bombarding a sample of interest with neutrons, e.g. from a radioisotopic neutron source, and monitoring the energies of the resulting prompt gamma-rays using an appropriate gamma-ray spectrometer in conjunction with a multi-channel analyzer (MCA). These prompt gamma-rays are characteristic of every element and of every isotope of every element. In addition, the neutron induced prompt gamma-rays can penetrate into substantial depths in the sample material as these have energies that range from few hundred keV up to 11-12 MeV. The above mentioned properties of the PGNAA method allow its utilization in cases where compositional/elemental analyses of bulk samples are required. It should also be made clear that the determination of the amounts of the constituents of a sample using the PGNAA method represents an inverse problem in the sense that the *cause(s)* of the *effect(s)* registered by the spectrometer has/have to be estimated. In a forward problem, the opposite would be the case.

[2] Even though the focus of this project is on the ***intrinsic gamma-ray stopping efficiency*** of GM counters, terms such as gamma-ray detection efficiency, gamma-ray stopping efficiency and gamma-ray efficiency will be used interchangeably throughout this text.

Recently, the feasibility of PGNAA method for determining the amounts of different components, i.e. oil, gas, water and salt, which may be found in an offshore multiphase flow was demonstrated successfully [5]. This recent development has prompted the consideration of the use of the PGNAA method for detailed characterization of produced water samples. Hence, the second project in this thesis work is the PGNAA method which is proposed as an alternative to the DMD principle for produced water characterization.

In the recent work by Wang et. al. [5] in which the feasibility of utilizing a PGNAA analyzer for determining the amounts of individual components of a multiphase flow was demonstrated, the so-called Monte Carlo library least-squares (MCLLS) approach [25-27] was used for the subsequent inverse quantitative analyses. Briefly, it can be mentioned that the MCLLS approach is used in order to take advantage of the information contained within the entire prompt gamma-ray spectrum of the sample by assuming that the total count rate in the total prompt gamma-ray spectrum of any sample can be given as the sum of the products of the amounts and the library spectrum of each constituent of the sample. The amounts of each constituent in the sample are then calculated in a least-squares sense using the sample spectrum and the library spectrum of each constituent of the sample. In chapter 3, a relatively detailed description of the MCLLS approach is given. The MCLLS approach was also the major quantitative analysis tool throughout the feasibility study presented in this thesis. As mentioned above, the MCLLS approach assumes that the library spectrum of each constituent of the sample is available prior to executing the least-squares search. Since the experimental generation of these library spectra would be a very tedious and time-consuming task, the MCLLS approach relies on very accurate forward MC calculations for this purpose. Therefore, the approach taken in the second project is to first carry out experiments in which a produced water sample prepared in the laboratory was bombarded by neutrons from a californium-252 (Cf-252) spontaneous fission neutron source. The energies of the resulting neutron induced prompt gamma-rays were then monitored using a large, 6 in. x 6 in. NaI(Tl) scintillation detector and a MCA. Secondly, in accordance with the MCLLS approach, a MC model of the measurement setup was developed in order to generate the library spectra of the constituents of the produced water sample. These library spectra, together with the experimental sample spectrum, were then used to determine the amount of each constituent.

An overview of the relevant physics of the PGNAA method as well as a detailed description of the PGNAA analyzer used to demonstrate the feasibility of applying the PGNAA method in the context of analyses of produced water samples is given in chapter 3 and paper 3. Moreover, sections 3.3.1, 3.3.2 and 3.3.3 of chapter 3 will be devoted to the MCLLS approach itself and its limitations. It can, however, be already stated here that a substantial limitation was identified to be the ill-conditioning in the MCLLS approach. In this thesis work, a new iterative method is proposed with the intention of improving the sensitivity of the MCLLS approach in such ill-conditioned cases. The proposed iterative method is then applied to the ill-conditioned multiphase flow measurement problem to demonstrate its feasibility. It can also be said that the new iterative method proposed in the work presented in this thesis could be interpreted as a modification of the already well-established MCLLS approach and is, therefore, one of the major contributions of this work.

The results of these analyses, a detailed description of the proposed iterative method as well as a discussion on the pertinent limitations of the MCLLS approach are given in chapter 3 and paper 4.

1.4 Introduction to MC simulations

This thesis work investigates the feasibility of utilizing GM counters in the DMD principle for the characterization of produced water samples as well as the feasibility of an alternative approach to the DMD principle, i.e. the PGNAA method in conjunction with the MCLLS approach. In both cases, the major computational tool was the MC simulation of radiation transport. This is mainly because the MC simulations provide a flexibility that can be difficult or impossible to achieve in laboratory experiments. MC simulations are not as time consuming and costly as experimental efforts, and may provide a better insight into the critical parameters related to the estimation of the physical quantities of interest, such as the gamma-ray stopping efficiencies of GM counters. The MC models developed in conjunction with the investigations regarding the above mentioned measurement systems were benchmarked with experimental data. The benchmarked MC models were then used to study different aspects of these measurement systems. Therefore, in this section, giving a very brief overview of MC simulations in the context of radiation transport is in order. More on the theory of MC simulations of radiation transport can be found in [28-30].

The MC simulations are a computational tool that may be used to provide an average value of a quantity of interest by iterative random sampling from appropriate distributions that describe the average behavior of that quantity. Therefore, it can be stated that the MC simulations are usually used for problems of stochastic nature, that is, problems that cannot be solved analytically. The transport of radiation through matter fits this description very well as the path a particle propagating through an absorber is decided based on the outcomes of a number of stochastic events.

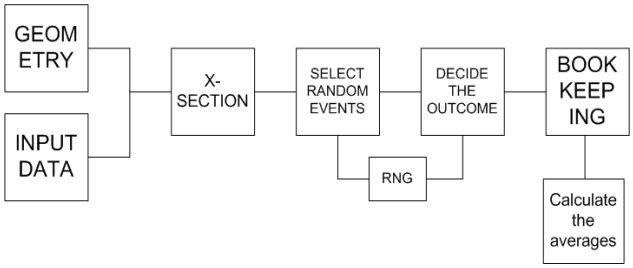

Figure 1.4 **A block diagram showing the pertinent elements of the MC simulation of radiation transport through an absorber. Here, RNG stands for "Random Number Generator".**

In figure 1.4, a block diagram presenting the pertinent elements of a MC simulation of radiation transport through an absorber is shown. The MC simulation will start with a definition of the problem geometry in which the average values of the quantities of interest will be calculated. The simulation will also require additional input data such as source definition and material definition. The pre-defined energy, type, coordinates and initial direction of primary particles, also referred to as the phasespace of primary particles, need to be provided prior to the execution of the simulation. Depending on the simulation package utilized, relevant materials will be assigned to different bodies/volumes defined in the problem geometry either while defining the problem geometry or through a separate input file. Generally, all MC simulation packages will require their users to provide such information. This is because the pre-defined problem geometry, input data and the appropriate cross-sectional data are used in conjunction with a proper random number generator (RNG) to select the outcome of a possible event in a random manner. The remainder of any MC simulation is considered to be bookkeeping where the appropriate particle counters are

incremented whenever an event of interest takes place, such as when a given type of particle crosses a given surface in the problem geometry. Finally, the averages of the quantities of interest are calculated once a given number of primary particle histories, i.e. from the moment the particle is generated until the particle has escaped or absorbed within the problem geometry, are simulated or the allocated simulation time is exhausted.

There are several available general purpose MC radiation transport simulation packages which implement different interaction models and different particle transport algorithms. FLUKA [31], EGS4 [32], GEANT4 [33], TART2005 [34], MCNP5 [35] and PENELOPE [36] can be listed as examples of general purpose MC codes. Most of these MC simulation packages are publicly available and their distribution is not restricted. Therefore, the user has the freedom to choose a simulation package that would be the most suitable to solve a problem of interest. During this thesis work, only two of these general purpose MC codes, i.e. MCNP5 and PENELOPE, were utilized as both MCNP5 and PENELOPE are capable of simulating photon/electron showers in arbitrary geometries and also due to the fact that both have been benchmarked with extensive experimental data by other users [37-41]. An introduction to these MC simulation packages will not be given here. Instead, the interested reader is referred to the relevant references. In addition to these general purpose codes, two specific purpose MC codes, GMMC (Geiger-Müller Monte Carlo) and CEARCPG (Center for Engineering Applications of Radioisotopes Coincidence Prompt Gamma-ray) [42, 43] were also utilized. In connection with the MC modeling of the response of cylindrical GM counters to low energy gamma-rays, the specific purpose MC code GMMC was developed and benchmarked with both experiments and simulated data obtained using MCNP5 and PENELOPE. The development of GMMC can also be considered to be one of the major contributions of this thesis work in the identification of a method whereby the gamma-ray detection efficiency in these detectors could be improved. On the other hand, CEARCPG is a specific purpose MC code developed by the members of CEAR (Center for Engineering Applications of Radioisotopes) at North Carolina State University, USA. The code CEARCPG is capable of simulating neutron induced prompt gamma-ray production in arbitrary geometries and materials as well as generating the elemental/component prompt gamma-ray libraries required in the MCLLS approach. More detailed description of the specific purpose MC code GMMC is given in chapter 2 whereas that of CEARCPG can be found in [42, 43].

2. GM counters in DMD measurements for produced water characterization

As mentioned in the introduction section of this thesis, the possible utilization of GM counters in the DMD measurements considered for produced water characterization will, to some extent, depend on a potential improvement of these counters' poor gamma-ray stopping efficiencies. In this chapter, the work done to investigate a method for this purpose is presented. First of all, a background of the work presented in this chapter is given. This is followed by a section on the MC modeling of a cylindrical GM counter using two general purpose MC codes, MCNP5 and PENELOPE. Next, a section is devoted to the specific purpose MC code GMMC which was developed for more accurate MC modeling of the low energy gamma-ray response of cylindrical GM counters. Finally, the method considered for the improvement of the intrinsic low energy gamma-ray stopping efficiencies in cylindrical GM counters is presented. Details of the calculations involved in this chapter are given in a series of papers (see papers 1, 2 and 5).

2.1 Background of the GM counter project

As pointed out earlier, one of the key measurement challenges in the SOFA concept is the characterization of produced water samples. Using the prototype of the SOFA concept, feasibility studies with the DMD measurement principle were carried out. The CdZnTe semiconductor detectors were used in these preliminary experimental and MC investigations mainly because these detectors can essentially detect all incident gamma-rays at the photon energy of interest, i.e. at 59.5 keV. Within short integration times, typically about 2 min. [10], this choice of detectors would allow much better statistical accuracy, i.e. higher SNR values, in the measurement results with respect to gas-filled GM counters.

In a semiconductor detector, the band gap, i.e. the energy gap between the valence band and the conduction band, is of the order of 1 eV [1]. This energy can also be achieved by thermal excitation of electrons. Moreover, the thermal excitation probability of electrons exhibit very strong temperature dependence [1]. The thermally excited electrons will cause a current to flow through the semiconductor material. This is basically unwanted noise and will reduce the SNR in the measurements. In the SOFA concept, the thermal excitation of electrons in the CdZnTe semiconductor detectors will not constitute a major challenge. This is because the temperature at the seabed will remain stable at about 4ºC. However, in case an equivalent instrument is to be used for downhole measurements, stable operation cannot be maintained using CdZnTe semiconductor detectors due to extremely high temperatures found in such hostile environments. In addition, the CdZnTe semiconductor detectors will be sensitive to mechanical vibrations due to their piezoelectric properties [1]. This would further contribute to the overall noise at the detector output even though the effects related to mechanical vibrations could be reduced or in some cases totally eliminated by placing these detectors in silicon rubber beds [1]. Utilizing CdZnTe semiconductor detectors is possibly a good solution in the DMD measurements employed in the SOFA concept due to their superior gamma-ray detection efficiencies. In spite of this, it would still be in the offshore industry's best interest to minimize maintenance costs which, in turn, requires the development and installation of measurement systems that are as robust and cost-effective as possible.

GM counters are gas-filled ionizing radiation detectors that can be used to detect gamma-rays, X-rays and charged particles. On the contrary to CdZnTe semiconductor detectors, the GM

counters exhibit a high degree of robustness in harsh environments such as those found in offshore subsea hydrocarbon production facilities. Usually, GM counters are constructed using a thin anode wire which is surrounded by a cylindrically shaped cathode wall. Primarily, thin anode wires are used to achieve high values of the electric field which is needed to generate the Geiger discharge. Depending on the type and energy of radiation to be detected, Geiger counters may exhibit some structural differences.

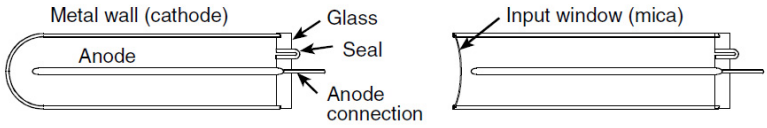

Figure 2.1 Typical GM counter geometries designed for detection of gamma-rays (left) and for detection of charged particles and low energy X-rays (right). The diameter of the anode wire is usually about 1.0 mm [1].

As shown in figure 2.1, some GM counters are constructed using thin radiation entrance windows. These are primarily used to detect charged particles and low energy X-rays whereas counters constructed using metal walls are used for detecting gamma-rays. However, GM counters with thin radiation entrance windows are more susceptible to damage and are not preferred in permanently installed industrial gauges. In addition, the thin radiation entrance windows are made of low density and atomic number materials (e.g., mica) in order to minimize attenuation of incident radiation in the entrance window. This would further reduce the sensitivity of the counter to incident gamma-rays as these will undergo collisions mostly within the solid parts of the counter instead of causing direct ionization of the fill gas. Moreover, it should also be mentioned that GM counters cannot be used in applications that require energy sensitive detectors. This is due to the mechanism of radiation detection in GM counters. More on the GM counters can be found in [1, 19, 20, 44].

In addition to their structural robustness, the fact that they require relatively simple read-out electronics, their relatively low costs, the availability of GM counters for operations up to 200 ºC and their insensitivity to mechanical vibrations have made their use an attractive option in many industrial gauges such as level, density and thickness gauging [1]. This is also because these are applications that do not require information on the type or energy of the detected radiation.

A sketch of the DMD measurement principle is shown in figure 2.2.

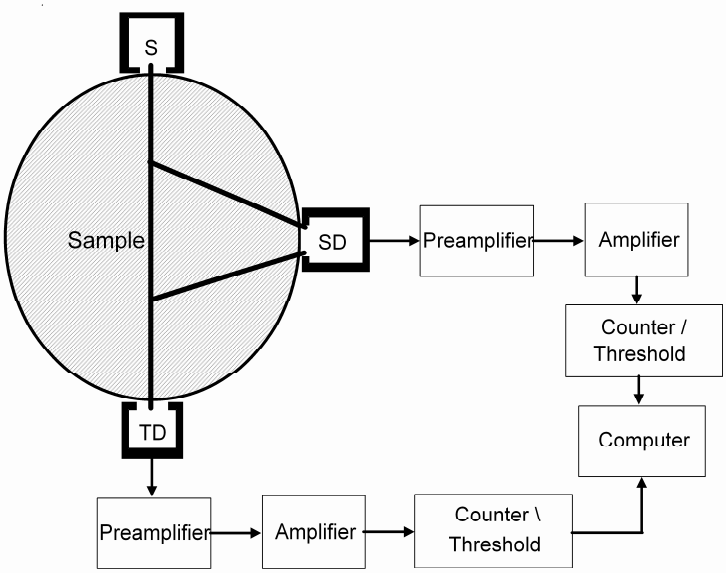

Figure 2.2 A sketch of the DMD measurement principle. S: source, SD: scatter detector and TD: transmission detector. Also shown in the figure is a block diagram of the read-out electronics for solid state, i.e. semiconductor or scintillation, detectors. For GM counters, use of the preamplifier and amplifier is not needed.

As shown in figure 2.2, the source is placed on the opposite side of the sample facing the transmission detector whereas the scatter detector is placed somewhere between the source and the transmission detector. These two detectors are used to monitor the integral number of transmitted and scattered source particles (in this case, photons). This property of the DMD approach supported by the above mentioned properties of GM counters have prompted an interest in the possible utilization of GM counters in the DMD measurement setup employed in the SOFA concept. However, there are some serious downsides to using GM counters that limit their applicability in many industrial process applications. GM counters exhibit extremely high inherent dead-times [1, 19, 20, 44]. This is basically due to the large number of ion pairs produced in the Geiger discharge mechanism. The significantly high dead-time in these detectors, in turn, limits their count-rate capabilities (approximately 10^4 counts/s). In most GM counters, the dead-time is about 50-100 μs [19, 44]. Their lifetime which is of the order of 10^{10} counts can also be pointed out as another limiting property. However, in a recent work, it has been shown that the count-rate capabilities of cylindrical GM counters could be improved by one order of magnitude by using a so-called active quenching technique in the read-out circuitry [45]. The technique is essentially based on automatically reducing the bias voltage in order to terminate the discharge process at an earlier stage and thus, reducing the detector dead-time. Another important downside to utilizing GM counters in industrial gauges is the fact that they exhibit relatively poor intrinsic gamma-ray detection efficiencies. These counters are known to have only about 1.0% detection efficiency over a wide range of

photon energies [1, 2, 19, 20]. This is mainly due to the fact that incident photons will penetrate the low density fill gas without causing any direct ionization. A major fraction of the counts will be generated through detection of secondary electrons created within the solid parts of the counter through photoelectric effect or Compton scattering. The low gamma-ray detection efficiency may lead to very low SNR values in the measurements when short integration times are desired. In addition, the poor gamma-ray detection efficiency may require the use of gamma-ray sources with higher activities which would be in disagreement with the ALARA principle.

In spite of the poor detection efficiencies, the utilization of GM counters in the DMD approach (and potentially in downhole instrumentation) may be realized provided that their gamma-ray detection efficiencies could be improved. Therefore, it was decided that the investigation of a method for this purpose, would have critical importance. Several different methods to improve the sensitivity of GM counters to incident gamma-rays have been proposed [2, 44]. In this thesis, the feasibility of a new method was studied through validated MC simulations. Previously, an analytical method for estimating the GM counters' gamma-ray stopping efficiency has been presented and applied for several counter configurations [46]. Also, the MC method was previously applied to the determination of the gamma-ray stopping efficiencies of cylindrical GM counters [47]. However, in both cases the focus has been on gamma-ray energies above 100 keV. Therefore, in the remainder of this chapter, the MC modeling of a specific type of GM counter, with emphasis on low energy gamma-rays, is discussed and the results are presented.

2.2 The GM counter

The study at hand was initiated by selecting a GM counter that would be most suitable in the DMD approach considered in the SOFA concept. It was decided to select the ZP1200 GM counter, manufactured by Centronic [20], as this is a versatile and robust GM counter with many industrial applications such as in the Tracerco Profiler™, which is a multiple source/detector system used for measurements of component phase levels as well as component densities in gravitational separators [48, 49]. Versions of the Tracerco Profiler™ employing ZP1200 GM counters are also available for subsea hydrocarbon production facilities. Also, the ZP1200 GM counter does not have a thin, low attenuation radiation entrance window which otherwise would make the counter more susceptible to damage in harsh environments.

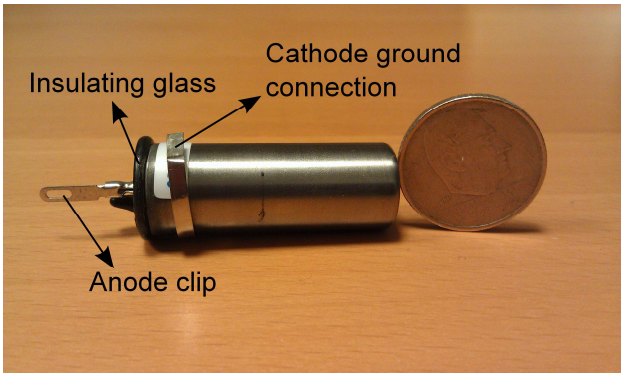

Figure 2.3 The Centronic ZP1200 GM counter used in this study.

In figure 2.3, a photograph of the ZP1200 GM counter is given. The counter used in the studies was supplied by Centronic. The fill gas of the ZP1200 counter is kept at a low value, about 135 mbar, in order to allow the formation of full Geiger discharge at relatively low bias voltages (of the order of 500V). This, in turn, leads to the fact that the intrinsic gamma-ray detection efficiency of ZP1200 counters depends on the efficiency by which the incident photons are converted to secondary electrons in the solid parts of the detector as well as on the efficiency by which these secondary electrons penetrate the solid parts and reach the fill gas. As discussed in paper 1, the latter depends on the electron's projected range [50], emission position and direction.

In the read-out circuitry, it is recommended by the manufacturer to keep the cathode of the counter at ground potential. The anode is then connected to the positive high voltage supply.

2.3 MC modeling with MCNP5 and PENELOPE

This chapter and paper 1 focuses on the MC modeling of the intrinsic low energy gamma-ray stopping efficiencies of the ZP1200 GM counter. This was performed by implementing MC models of the ZP1200 counter using two general purpose MC codes, MCNP5 and PENELOPE. The results of the MC simulations were then benchmarked with the previously obtained experimental stopping efficiency data [2].

The steps taken in the MC modeling with MCNP5 and PENELOPE as well as the MC generated results are illustrated in a much more detailed manner in paper 1.

2.3.1 Experiments

The experimental measurement geometry was based on illuminating the ZP1200 counter from the front with a well-collimated 59.5 keV gamma-ray beam [2]. A sketch of the measurement geometry is given in figure 2.4.

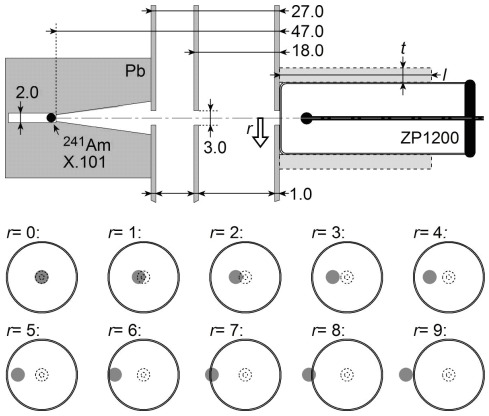

Figure 2.4 **The measurement geometry used in the experimental study. The same geometry was implemented in the MC simulations with the ZP1200 GM counter. As shown here, the beam was moved from the center of the detector toward the cathode wall in steps of 1 mm, from r = 0 mm to r = 9 mm. The shaded circle is the beam and the dashed circles are the anode wire and its tip bead. All dimensions are given in mm.**

In the experiments, the reference measurements were carried out using a 10 x 10 x 3 mm^3 CdZnTe semiconductor detector as this detector has essentially 100% gamma-ray stopping efficiency at 59.5 keV. The associated detector read-out electronics for both the CdZnTe detector and ZP1200 GM counter are described in paper 1.

2.3.2 MC modeling

The measurement geometry shown in figure 2.4 was modeled using MCNP5 and PENELOPE. The development of the MC models as well as the experiments was based on illuminating the counter from the front and moving the incident beam gradually toward the cathode wall in steps of 1.0 mm from r = 0.0 mm to r = 9.0 mm. In any MC simulation, it is of critical importance to use the correct detector dimensions and material composition for benchmarking purposes. Therefore, the manufacturer supplied material composition data were utilized. This and the pertinent detector dimensions are given in paper 1. Also, in the MCNP5 model as well as in the experiments, possible effects of encapsulating the counter with aluminum and tin casings on its gamma-ray stopping efficiency were investigated.

2.3.3 Results

The MC simulated and experimental gamma-ray stopping efficiency curves of the ZP1200 GM counter as a function of the radial beam position are given in figure 2.5

As pointed out in paper 1, the most obvious observation that can be made in figure 2.5 is the significant deviation of the simulated stopping efficiency curves from the experimental one as well as the detector's extreme sensitivity to its positioning with respect to the incident photon beam (see the error bar at r = 5.0 mm in figure 2.5). Also, it was pointed out that covering the outer surface of the GM counter with metal casings only has marginal effects on its gamma-ray stopping efficiencies whereas the large variations in the experimental results are most likely due to mounting, repeatability and positioning issues.

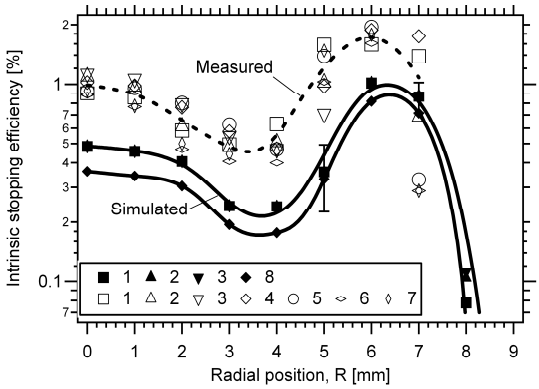

Figure 2.5 Simulated (solid legends and best fit curve) and experimental (open legends and dashed best fit curve) intrinsic gamma-ray stopping efficiency as a function of radial position of the 3 mm diameter beam. The numbers next to the legends represent: 1) Bare GM counter measured and simulated using MCNP5, 8) Bare GM counter simulated using PENELOPE and further GM counter surrounded by tubes of the following material and dimensions (length×thickness in mm): 2) Al (15×3), 3) Al (32×3), 4) Al (15×3) with cone opening, 5) Al (15×9), 6) Sn (15×5), and 7) Sn (15×2). Case 4) is similar to case 2) except that the covering tube has a cone inner opening in the front. The error bars shown on the simulation results of the bare GM counter is the effect of tilting the beam by 0.5° toward the anode and the cathode of the counter.

2.3.4 Discussions on MCNP5 and PENELOPE results

In paper 1, possible mechanisms that may be the cause of the substantial deviation between the simulated and experimental stopping efficiencies are investigated and discussed in detail. In summary, the following have been identified;

- the use of condensed history (CH) technique in MCNP5 [35] which makes use of the straight line approximation,
- the use of generalized oscillator strength (GOS) approach for simulating inelastic collisions of electrons in PENELOPE [36] which groups the contributions from the outermost shells into a single delta oscillator,
- the surface porosity of the chromium (Cr) coating that is plated onto the inner cathode walls of the ZP1200 GM counter.

Of the three points given above, the effect of the surface porosity of Cr coating on the MC simulations is common to both MCNP5 and PENELOPE models and was identified to be the major cause of the underestimated low-energy gamma-ray stopping efficiencies. This is mainly because the surface porosity of the Cr coating increases the inner surface area of the cathode walls. For low energy electrons, this means that the probability of secondary electrons to penetrate the cathode walls and reach the fill gas will be somewhat higher than the MC simulated one. This observation was confirmed through MC simulations where the surface porosity of the Cr coating was modeled using of saw tooth surfaces (see paper 1). In line with the expectations, it was observed that increasing the inner surface area of the cathode walls leads to a corresponding increase in the number of secondary electrons that penetrate the inner cathode walls and reach the fill gas. Using saw tooth surfaces was, however, identified to be a computationally inefficient way of taking into account the surface porosity of the Cr coating in the MC simulations. In an earlier work with the aim of simulating accurate NaI detector response functions (DRFs), use of density multiplication factors was evaluated to account for the effect of electron channeling in NaI crystals [51]. This factor would reduce the density of the NaI crystal for electron transport and increase the electron loss in the simulations. The successful application of this approach in simulating NaI DRFs, together with the fact that the implementation of the surface porosity of the Cr coating in the MC simulations had no appreciable effect on the photon transport through this structure, prompted an interest in pursuing a similar approach in MC modeling of GM counters. Using PENELOPE, MC simulations were repeated for several different density multiplication factors and the best density multiplication factor was found through a chi-square test of distributions [52].

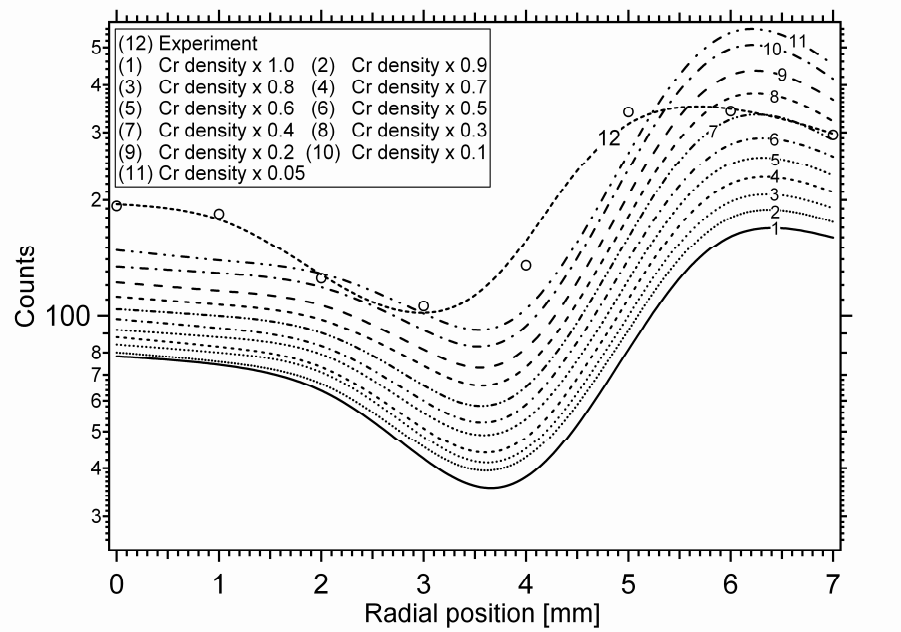

Figure 2.6 **Simulated stopping efficiencies for different density multipliers (best fit lines from (1) to (11)), ranging from 1.0 to 0.05, using PENELOPE and experimental (open legends and the dashed best fit curve, (12)) stopping efficiencies of the ZP1200 GM counter as a function of the radial beam position relative to the center of the detector.**

The results shown in figure 2.6 (where stopping efficiency curves are plotted as a function of various density multiplication factors) and the results of the reduced chi-square analysis yielded a density multiplication factor of about 0.4 – 0.3 where the minimum reduced chi-square value of 41.62 was obtained.

In addition, as mentioned above and discussed in paper 1, the possible effects of the treatment of electron transport in MCNP5 and PENELOPE were to be investigated. As stated in paper 1, this could only be achieved through comparison between MCNP5 and PENELOPE simulated stopping efficiency curves and those that are obtained using a MC code that employs electron transport simulation on an event-by-event basis (also referred to as the single scatter approach [53, 54]) as well as experimental stopping efficiencies. This would also enable more accurate MC modeling of the intrinsic gamma-ray stopping efficiency in cylindrical GM counters.

2.4 The single scatter electron Monte Carlo approach

In this section, to be able to justify the statements made in the previous section, the focus is on the development of a specific purpose MC code called GMMC (Geiger Müller Monte Carlo) that employs detailed simulation of electron transport. In the remainder of this section, a more elaborate description of the GMMC code will be given whereas the results of benchmark experiments will be briefly described. More details on the benchmark experiments can be found in paper 2.

2.4.1 The specific purpose MC code GMMC

It has been shown that, especially in thin geometries and at low electron energies, the detailed simulation of electron transport (also referred to as the single scatter approach, microscopic or analog electron simulation) in absorbers provides more accurate results in comparison with general purpose MC codes that employ the CH technique for accelerated simulation of electron transport [54]. The inaccuracies in the electron transport when the CH technique is utilized are usually attributed to the use of (a) multiple scattering angular distributions, (b) multiple scattering energy loss distributions and (c) the straight line approximation [54]. The reader is referred to [53, 54] for a comprehensive discussion on the impact of these mechanisms on the results of low energy electron transport through absorbers.

Due to the reasons mentioned above and the MC simulated results presented in the previous section, it was decided to pursue the development of a specific purpose MC code, so-called GMMC, that employs the single scatter electron transport technique in spite of the technique's computational inefficiency. This is a direct result of the fact that detailed treatment of the electron transport within the solid parts of the ZP1200 counter would help eliminate any unwanted bias/distortions that might have been introduced through the approximations involved in the CH technique or the approximations contained within the GOS approach utilized in the MC code PENELOPE to treat the electron inelastic scattering events (see section 2.3.4 and paper 1).

The MC code GMMC is capable of simulating coupled photon/electron transport, and it utilizes the above mentioned single scatter technique for electron transport. GMMC was developed on a linux platform using the fortran 90 programming language which is a standard programming language frequently used in computational physics. In addition, GMMC was written as a collection of several subroutines, and compiled using the intel fortran 11.1 compiler for linux. A list of the GMMC subroutines is given in appendix 1. A flowchart showing the pertinent processes in the GMMC code is given in figure 2.7 whereas the specific geometry of the ZP1200 GM counter is hard-coded into the MC code.

The GMMC simulation of the low energy gamma-ray intrinsic stopping efficiency of the ZP1200 counter starts with sampling the so-called phasespace of the source particle. That is, the energy, E, of the source particle is set, which in this case is only a monoenergetic source with emission energy of 59.5 keV. Also, the Cartesian position coordinates, x, y and z are either set equal to predefined values or sampled from appropriate distributions. Moreover, the predefined polar, θ, and azimuthal ,φ, angles were used to calculate the direction cosines u (along x-axis), v (along y-axis) and w (along z-axis) of each source particle according to:

$$\left.\begin{aligned} u &= \sin\theta\cos\varphi \\ v &= \sin\theta\sin\varphi \\ w &= \cos\theta \end{aligned}\right\} \begin{aligned} &\theta : [0, \pi] \\ &\varphi : [0, 2\pi] \end{aligned} \qquad (2.1)$$

where, for an isotropic source, θ and φ are distributed uniformly between $[0,\pi]$ and $[0,2\pi]$, respectively.

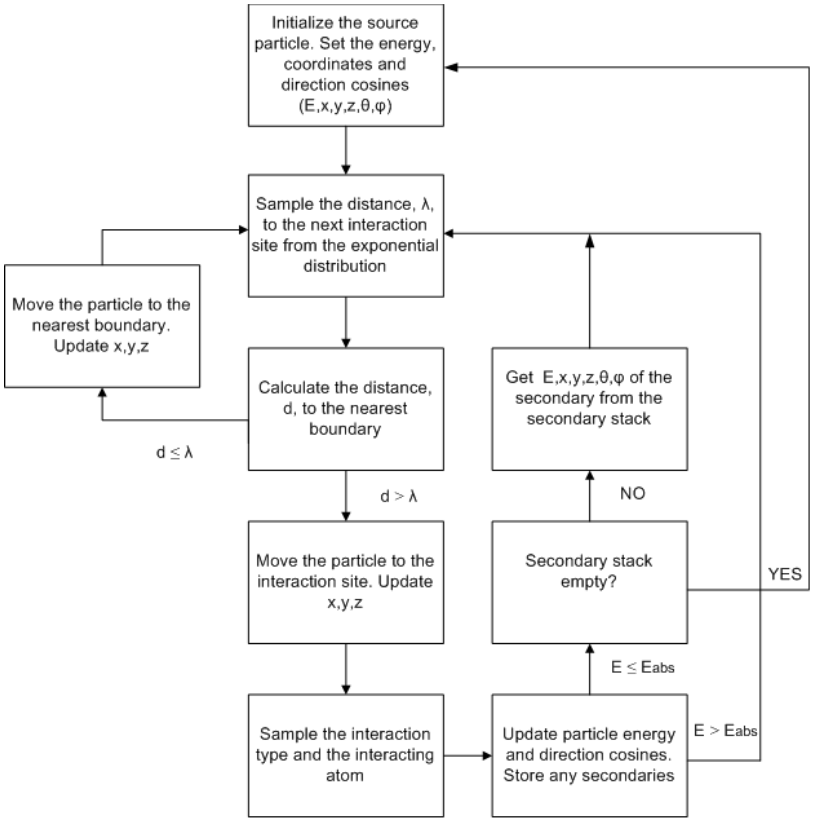

Figure 2.7 A flowchart showing the important steps of the GMMC code. Not shown in this flowchart is the step where the transport of secondary electrons is terminated upon detection in the fill gas. Also, the two variance reduction techniques employed in GMMC are not shown explicitly (see section 2.4.5). In the figure, *x*, *y* and *z* are the Cartesian coordinates of the particle, *E* is the energy of the particle, θ and φ are the polar and azimuthal angles, respectively.

Once the sampling of the phasespace of a source particle is completed, a subroutine checks its distance to the surface of the detector and immediately moves the particle to the detector surface. At this point, the source particle's distance, λ, to the interaction site is sampled from the usual exponential distribution:

$$\left.\lambda = -\ln(\rho)\frac{1}{\Sigma}\right\} \qquad \rho : [0,1] \tag{2.2}$$

where Σ is the macroscopic cross-section given in cm^{-1} and ρ is a random number uniformly distributed between 0 and 1. The macroscopic cross-section Σ is given as; $\Sigma = N\sigma$ where N is the density of the nuclei (atomic density) in cm^{-3} and σ is the microscopic cross-section in cm^2 in a given absorber. After that, the particle's position coordinates are updated based on the sampled distance to the collision site in the absorber and the direction cosines of the particle. Mathematically, this can be shown as follows:

$$\begin{aligned} x &= x_0 + u\lambda \\ y &= y_0 + v\lambda \\ z &= z_0 + w\lambda \end{aligned} \tag{2.3}$$

where x_0, y_0 and z_0 are the original position coordinates of the particle. It should, however, be mentioned that the sampled distance to the interaction site will have to be compared to the distance to the closest material interface on the path of the particle prior to updating the particle position coordinates. Care must be taken if the interaction distance sampled from the exponential distribution is greater than the distance to the nearest interface. In GMMC, the procedure is; (1) move the particle to the interface; (2) stop the simulation at the interface and (3) sample a new λ using the cross-sectional data of the new material.

Once the particle coordinates are updated, the collision type is sampled. Additionally, the colliding element had to be sampled as well as the collision type in cases where the volume in which the particle is propagating is made up of a mixture of elements. The collision type is sampled using the macroscopic interaction cross-sections. In case of simulation of low energy photon transport (where there is no contribution from pair production events) this can be formulated as follows:

$$\begin{aligned} &\text{(a)} \quad \rho \le \frac{\Sigma_{pe}}{\Sigma_t} \\ &\text{(b)} \quad \frac{\Sigma_{pe}}{\Sigma_t} < \rho \le \frac{\Sigma_{pe} + \Sigma_{Co}}{\Sigma_t} \\ &\text{(c)} \quad \frac{\Sigma_{pe} + \Sigma_{Co}}{\Sigma_t} < \rho \le \frac{\Sigma_{pe} + \Sigma_{Co} + \Sigma_{Ra}}{\Sigma_t} \end{aligned} \tag{2.4}$$

where ρ is a random number uniformly distributed between 0 and 1, Σ_{pe} is the macroscopic photoelectric absorption cross-section, Σ_{Co} is the macroscopic Compton scattering cross-section, Σ_{Ra} is the macroscopic Rayleigh scattering cross-section and Σ_t is the macroscopic total interaction cross-section in a given material.

The colliding element in a material consisting of several elements was sampled based on the atomic fractions of the individual elements. Normally, the weight fractions of each constituent in the material and the material density are provided as input in MC simulations. In these cases, the atomic densities are calculated according to [55]:

$$N_i = \frac{\rho_{material} w_i N_A}{A_i} \tag{2.5}$$

where N_i is the atomic density of the i^{th} element given in [atoms/cm^3], w_i is the weight fraction of the i^{th} element, $\rho_{material}$ is the mixture density, A_i is the atomic weight of the i^{th} element in the material and N_A is Avogadro's number which equals 0.6022 $\text{atoms}\frac{\text{cm}^2}{\text{mol}\cdot\text{barn}}$. Then the atomic fractions of the individual constituents in the material are calculated as:

$$a_i = \frac{N_i}{\sum_{i=1}^{n} N_i} \tag{2.6}$$

where a_i is the atomic fraction of the i^{th} element in a given mixture. The elemental microscopic cross-sections are then weighted by the atomic fractions to obtain the macroscopic cross-sections of each element. If, for instance, a Compton scattering event is sampled then the Compton scattering macroscopic cross-sections are used to sample the colliding element in a similar fashion to the sampling procedure described for the sampling of the collision type.

Once the collision type and the colliding element are determined, GMMC checks whether or not any secondary particles are produced in the collision being simulated. At the moment, GMMC simulates only photoelectrons and ignores the simulation of other secondary particles produced in e.g., Compton scattering and electron ionization events. Therefore, this check is performed only when a photoelectric event takes place. Thereafter, GMMC stores the phasespace parameters of photoelectrons in the secondary stack.

The energy and direction cosines of the particle are updated where necessary and a new distance to the next collision site is sampled from the exponential distribution. The simulation procedure described so far is also referred to as analog MC simulation as every collision the particle suffers is simulated individually. The analog MC simulation is mostly applied to simulation of photons through absorbers. This is because photons, on the average, travel relatively significant distances between two successive collisions in an absorber, and undergo collisions relatively infrequently. On the other hand, as far as simulation of charged particles is concerned, this procedure is very often avoided in many general purpose MC codes due to extremely short distances charged particles travel between two successive collisions. In addition, charged particles may suffer a significantly large number of collisions prior to being absorbed in the material or termination of their simulation due to other reasons. However, it should also be kept in mind that the procedures described so far are the basis of the single scatter electron transport approach.

A few words regarding the random number generator (RNG) used in GMMC are also in order. Use of a validated, stable and long period RNG is of crucial importance in any calculation based on the MC method. For this purpose, the RNG currently employed in PENELOPE [36] was used in GMMC. This RNG was originally proposed by L'Ecuyer [56]. It has a very long period which is of the order of 10^{18}. A fortran 90 implementation of this RNG is given in appendix 2.

In the next two subsections, the MC modeling of photon and electron interactions in GMMC will be briefly described.

2.4.2 Modeling of photon interactions in GMMC

In GMMC, all photon interactions are modeled with the exception of pair production. This is because the specific purpose MC code GMMC was developed in order to study the gamma-ray intrinsic stopping efficiency of the ZP1200 GM counter at primary photon energy of 59.5 keV. At this energy, the pair production event cannot take place as its threshold energy is at 1022 keV. Although adjustable, the photon cut-off energy was set equal to 1.0 keV. In this

section, a brief overview of the photon sampling procedures employed in GMMC will be given. For more comprehensive reading, the reader is referred to the references [28-36]. It should also be mentioned that the photo-atomic interaction data were extracted from the EPDL97 database [57] provided in the ENDF-6 format. For the ease of data processing and avoiding unnecessary data formatting, the MC code GMMC was programmed so as to allow direct access to cross-sectional data in the ENDF-6 format.

Rayleigh scattering becomes one of the predominant photon interaction mechanisms at low energies (< 10 keV). In Rayleigh scattering, the incoming photon is deflected upon collision with the target atom. However, there is no energy transfer in this process. The target atom is left in its original, unexcited state. Since the incoming photon scatters from all electrons coherently, Rayleigh scattering is also referred to as "coherent" scattering. As there is no energy transfer in this interaction mechanism, only the scattering angle, θ, was sampled. This was achieved by sampling from the usual differential Thomson scattering-cross section:

$$\frac{d\sigma_T}{d\Omega} = \frac{1+\cos^2\theta}{2} r_0^2 \tag{2.7}$$

where $r_0 = 2.818 \times 10^{-13}$cm is the classical electron radius and Ω is the unit solid angle in the direction of the scattered photon. However, the classical Thomson scattering cross-section describes photon scattering on a single isolated electron. To take into account the scattering from *Z* electrons, the classical Thomson scattering cross-section is modified by an atomic form factor *F(q)* which is a function of the momentum q transferred to the atom. Then the modified differential cross-section can be written as:

$$\frac{d\sigma}{d\Omega} = \frac{d\sigma_T}{d\Omega} F(q)^2 \tag{2.8}$$

where the atomic form factor *F(q)* decreases the usual Thomson scattering cross-section more extremely for backscattering [35]. In the MC code GMMC this was achieved by rejecting or accepting a sampled scattering angle based on the pertinent atomic form factors.

Compton, or incoherent, scattering is different from Rayleigh scattering in the sense that the incoming photon collides with one of the bound electrons of an atom rather than interacting coherently with an atom as a whole. In this process, the incoming photon loses a certain fraction of its energy to the bound electron. The electron (referred to as Compton recoil electron) is then ejected from the atom with energy equal to the energy transferred by the incident photon minus the binding energy. Therefore, it is necessary to sample both the scattering angle, θ, and the energy lost by the incident photon when a Compton scattering event is sampled during the MC calculations. In GMMC, the sampling of these quantities is achieved through sampling from the usual Klein-Nishina differential cross-section which is given as:

$$\frac{d\sigma_{KN}}{d\Omega} = \frac{r_0^2}{2} \frac{1}{[1+\alpha(1-\cos\theta)]^2} \left[1+\cos^2\theta + \frac{\alpha^2(1-\cos\theta)^2}{1+\alpha(1-\cos\theta)} \right] \tag{2.9}$$

where Ω is the unit solid angle in the direction of the scattered photon, r_0 is the classical electron radius, $\alpha = E_\gamma / m_0 c^2$, i.e. the ratio of the incoming photon energy to the electron rest

mass energy and θ is the scattering angle. Sampling from the Klein-Nishina distribution is achieved through implementation of Kahn's method [58] in GMMC. Kahn's method was chosen as this is the recommended sampling procedure for exact sampling from the Klein-Nishina distribution for photon energies below 1500 keV [35]. A flow diagram showing the pertinent steps of Kahn's method is provided in figure 2.8 without providing a proof.

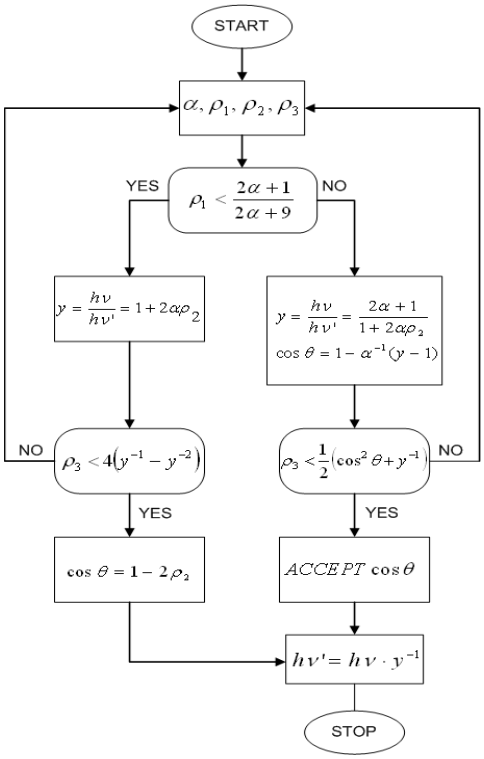

Figure 2.8 Flow diagram showing Kahn's method to sample the scattered photon energy from the Klein-Nishina differential cross-section [58]. Here, $\alpha = E / m_0c^2$, i.e. the ratio of the energy of the incident photon to the electron rest mass energy, ρ_1, ρ_2 and ρ_3 are three random numbers from 0 to 1 and $h\nu'$ is the energy of the scattered photon whereas $h\nu$ is the energy of the incident photon.

The Klein-Nishina differential cross-section describes scattering of photons on free electrons at rest. However, this assumption does not hold especially at low photon energies. To take into account the effects of electron binding energy, the Klein-Nishina cross-section is modified by the so-called incoherent scattering functions. Then, the differential scattering cross-section from a single, bound electron can be given as follows:

$$\frac{d\sigma_{atom}}{d\Omega} = \frac{d\sigma_{KN}}{d\Omega} S(q, Z) \tag{2.10}$$

where *S(q,Z)* is the so-called incoherent scattering function which decreases the conventional Klein-Nishina differential scattering cross-section more extremely in the forward direction and *q* is the again the momentum transferred to the target. In GMMC, the scattered photon energy and angle are, as mentioned above, sampled using Kahn's method and the sampled

scattering angle is then accepted or rejected according to the appropriate incoherent scattering function.

At 59.5 keV, the major contribution to the overall gamma-ray stopping efficiency of the ZP1200 GM counter will come from the photoelectric absorption events. In the photoelectric absorption, the incoming photon will transfer all of its energy to the target electron, which is followed by the termination of the simulation of the incident photon. The target electron will then be ejected from the atom with energy equal to the difference between the energy of the incident photon and the binding energy of the particular atomic shell. The EPDL97 photo-atomic database provides the photoionization subshell cross-section data of all elements. GMMC makes use of these data to determine atomic shell in which the photoelectric absorption will take place. The emission direction of the photoelectron will obey the Sauter differential cross-section which is given as [59]:

$$\frac{d\sigma}{d\Omega} \approx \frac{\sin^2\theta}{(1-\beta\cos\theta)^4}\left[\frac{1}{\gamma}+\frac{1}{2}(\gamma-1)(\gamma-2)(1-\beta\cos\theta)\right] \tag{2.11}$$

where $\beta = v/c$ of the electron, $\gamma = (1-\beta^2)^{-1/2}$ is the electron relativistic factor and θ is the polar angle at which the photoelectron is emitted. It should, however, be kept in mind that the effects of electron binding energies are omitted in the Sauter distribution. Nevertheless, it has been shown that sampling of the photoelectron emission angle from the Sauter differential cross-section does not introduce significant errors [36]. The MC simulation package PENELOPE employs a sampling scheme based on the rejection technique for sampling the emission directions of photoelectrons from the Sauter distribution which also is implemented in GMMC.

At the moment, however, GMMC neglects the simulation of atomic relaxations which involve production of characteristic X-rays (also referred to as radiative relaxation), Coster-Kronig and Auger electrons (also referred to as non-radiative relaxation). Of these, simulation of characteristic X-rays may prove to be a critical parameter in the determination of intrinsic gamma-ray stopping efficiencies of GM counters. Neglecting the simulation of characteristic X-rays may lead to inaccuracies in the MC simulations. Nevertheless, it is believed that this would not have a great impact on the MC simulated gamma-ray stopping efficiencies of GM counters as, at 59.5 keV, a significant fraction of secondary electrons reaching the fill gas and contributing to the final result are photoelectrons.

2.4.3 Modeling of electron interactions in GMMC

As opposed to many general purpose MC codes, the specific purpose MC code GMMC implements the single scatter technique for electron transport, i.e. GMMC employs detailed simulation of electron transport through absorbers. GMMC uses the electro-atomic cross-section data provided in the EEDL database [60]. These data are also provided in the ENDF-6 format. Although flexible, the electron transport simulation cut-off energy was also set equal to 1.0 keV as in the case of photon transport. In this section, a short overview of the treatment of electron transport in GMMC will be given. It should also be mentioned that much of the electron transport modeling follows that of CREEP, a single scatter MC code written for reliable low-energy electron transport in arbitrary media [53]. Use of CREEP was, however, not considered in the work presented in this thesis due to the fact that it does not treat coupled photon/electron transport through absorbers; that CREEP is capable of only simulating

electron transport in simple slab geometries as well as due to issues related to limited availability. For more comprehensive reading on electro-atomic interactions and their MC modeling, the interested reader is referred to [31-36, 53.].

In GMMC, elastic scattering, ionization and excitation events are taken into consideration. Also, the contribution from Bremsstrahlung events to the total electron stopping power (-dE/dx) is considered even though the simulation of Bremsstrahlung photons is omitted.

In elastic scattering events, the incoming electron scatters off of a nucleus without any appreciable energy loss. The EEDL database provides the elastic scattering angular distributions of electrons as a function of electron kinetic energy. GMMC calculates the scattering angle of electrons by sampling from these distributions using the rejection technique. The EEDL database, however, sets the transition point between large-angle and small-angle scattering at 0.081º, and does not tabulate the small-angle scattering differential cross-sections. The small-angle scattering differential cross-sections are, therefore, calculated internally by GMMC according to [59]:

$$\frac{d\sigma}{d\Omega} = \left(\frac{Zr_0}{\gamma\beta^2}\right)^2 \frac{1-\beta^2 \sin^2\frac{1}{2}\theta}{\left(1-\cos\theta+\frac{1}{2}\theta_s^2\right)^2} \tag{2.12}$$

where Z is the atomic number of the colliding atom and θ_s is the screening angle which prevents the differential scattering cross-section from diverging in the forward direction. Especially at low energies the screening effect becomes an important parameter and, as suggested in the EEDL database, Seltzer's semi-empirical expression for the screening angle is used to calculate its value [59]:

$$\theta_s^2 = \frac{\alpha^2}{\gamma^2\beta^2}\left(\frac{a_0}{a}\right)^2\left[1.13+3.76(\alpha Z/\beta)^2\left(\frac{E}{E+mc^2}\right)^{1/2}\right] \tag{2.13}$$

where a is the so-called screening distance which is comparable to the atomic radius and a_0 is the Bohr radius. The ratio of the Bohr radius to the screening distance is then determined based on the Thomas-Fermi model of the atom [59].

In excitation interactions, the incoming electron transfers some of its energy to the atomic electron raising it to an excited state. The incident electron will then continue propagating through the medium with reduced energy. The EEDL database provides tabulated average electron energy loss in excitation events. GMMC uses the average excitation electron energy loss data given in EEDL to determine the amount of energy transferred from the incident electron to the target atomic electron. At the energy of interest, i.e. at about 59.5 keV, this is only about 10 eV per excitation interaction. Following an excitation event, the incident electron is then assumed to continue its propagation along the same path without suffering any deflections. This is in accordance with the approximations employed in the EEDL database [60]. It was assumed that the inaccuracies that may be introduced through neglecting the angular deflection of electrons in excitation events would have a negligible effect on the spatial distribution of electrons. This is because the initial direction of electrons will mostly be modified by elastic scattering events.

In the ionization interactions, the incident electron knocks-out an atomic electron and thereby, ionizes the target atom. Ignoring the binding energy of the electron, the electron that is knocked-out from the atom can have energy from 0 to E/2, i.e. from 0 to half the energy of the incident electron. The two electrons emitted from the interaction site are indistinguishable and therefore, the more energetic one is considered to be the incident electron. Similar to the sampling scheme employed in CREEP [53], GMMC utilizes the ionization subshell energy spectra provided in the EEDL database to calculate the energy of the secondary knock-on electrons. Once the sampling of the knock-on electron energy is completed, energy of the incident electron is updated as:

$$E' = E - E_{ko} - E_{bj} \tag{2.14}$$

where $E`$ is the energy of the incident electron exiting the ionization collision, E is the energy of the incident electron prior to the ionization collision, E_{ko} is the energy of the knock-on electron and E_{bj} is the binding energy of the j^{th} atomic shell. The most energetic secondary electrons produced in ionization events are also referred to as delta-rays (δ-rays). These may also penetrate into appreciable depths in the absorber due to their relatively high energies. However, GMMC does not take into account the simulations of these δ–rays at this time. This is because incident electrons will have a much greater probability of producing many low-energy knock-on electrons. In addition to losing a fraction of its energy, the incident electron will be deflected in an ionization event. In a similar manner to the calculations performed in [53], the scattering angle of the incident electron is calculated using the two-body kinematics in which the binding energy of the target electron is assumed to be negligible:

$$\begin{aligned} R &= \frac{E - E'}{E} \\ \mu &= \left(R\left[\frac{E + 2E_0}{E - E' + 2E_0} \right] \right)^{1/2} \end{aligned} \tag{2.15}$$

where μ is the cosine of the scattering angle θ with respect to the direction of the incident electron, E is the energy of the incident electron, $E`$ is the energy of the knock-on electron and E_0 is the electron rest energy. Since the electron binding energies are ignored, these angles are, as stated in [53], expected to be less valid at energies of the order of the binding energies.

As in the case of photoelectric effect or Compton scattering events, the target atom is left in an excited state with a vacancy in one of its shells following an electron ionization event. This vacancy may be filled through a cascade of events where characteristic X-rays, Auger or Coster-Kronig electrons may be emitted. However, as mentioned in section 2.4.2, GMMC does not treat atomic relaxations at this time.

Bremsstrahlung is the process in which the incident electron is deflected from a nucleus or an atomic electron. During this process, the incident electron may be briefly accelerated due to the interaction of the Coulomb fields and may emit radiation (photons). The total electron stopping power is usually split into two; the collisional stopping power which is due to excitation and ionization events and the radiative stopping power which is due to Bremsstrahlung events. At the energy of interest, i.e. at 59.5 keV, the contribution from the radiative stopping power to the total stopping power of electrons in the materials of interest is negligible. At 59.5 keV, the Bremsstrahlung cross-section in, e.g., Cr, is about four orders of

magnitude smaller than the ionization cross-section. Therefore, it was decided to implement the treatment of Bremsstrahlung events in GMMC in a simplistic manner. The EEDL database provides the average electron energy loss in Bremsstrahlung events. The tabulated average energy loss data are utilized when a Bremsstrahlung event is sampled in the course of the simulation of the electron path. The secondary photons are not simulated. The incident electron is assumed to continue its propagation along its original path. However, as mentioned above, due to the insignificant contribution from Bremsstrahlung to the total stopping power of electrons at 59.5 keV, the possible effect of this assumption on the results of the MC calculations is expected to be negligible.

2.4.4 Geometrical operations in GMMC

In GMMC, the geometrical operations are handled internally. As mentioned in section 2.4.1, the specific geometry of the ZP1200 counter is hard-coded into GMMC through the use of appropriate quadratic equations that describe the volumes of interest. Also, as mentioned in section 2.4.1, it is crucial to check the volume in which the particle is propagating as well as checking its distance to the nearest boundary after sampling the distance to the next collision site. In GMMC, this is carried out by solving simultaneously for the appropriate quadratic equations [28] that describe the volumes on the particle path and for the straight line along which the particle is propagating. In this process, positive solutions to the quadratic equations will be obtained as well as negative solutions. The physical meaning of a positive solution is that the particle is approaching an interface whereas the meaning of a negative solution is that the particle is propagating away from an interface. In some circumstances, the solution may not exist indicating the fact that the extension of the particle's path will not cross any of the geometric boundaries. Furthermore, the minimum of all of the positive solutions will yield the distance to the nearest boundary the particle will cross unless it suffers a collision before reaching the boundary. A calculation example is given in appendix 3.

2.4.5 Variance reduction in GMMC

As discussed in section 2.4.1, simulating electron transport on an event-by-event basis is computationally inefficient. However, analog simulation of electron transport has the potential to mimic more closely the physical processes involved in the determination of the intrinsic gamma-ray stopping efficiencies of GM counters. As described in paper 1, the use of range rejection technique for electron transport in the solid parts of the GM counter was considered in the MCNP5 model of the counter. This is also the most efficient variance reduction technique that could be employed in the MC modeling of a gaseous detector. To improve the computational efficiency, the range rejection technique was also implemented in GMMC through the use of a separate subroutine that checks the distance from the current position of a secondary electron to the closest structure/fill gas boundary. The simulation of secondary electrons is terminated whenever the distance from their position to the nearest fill gas interface is more than 50 μm. Otherwise; the simulation of secondary electrons is continued in the usual way as explained in section 2.4.1.

Source biasing technique was also considered. This is because it could occasionally be more likely that a certain fraction of source particles distributed over space, energy and angle will contribute more to the result of the MC simulations [28]. In MC modeling of a cylindrical GM counter where the source is placed in front of the detector, there would not be much sense in simulating a source with isotropic emission. The source biasing technique was therefore

utilized to confine the source particles within a solid angle to define a cone beam. The statistical weight of each source particle was then adjusted as follows:

$$\omega = \omega_0 \frac{\int_0^{2\pi} d\varphi \int_0^{\theta} \sin\theta d\theta}{4\pi} \tag{2.16}$$

where φ is the azimuthal angle, ω is the adjusted weight of the source particle, ω_0 is the original weight of the source particle which equals 1.0 in purely analog calculations and θ is the half cone-angle. As can be seen from equation (2.16), the statistical weight of the source particles will remain unaltered when the emission is isotropic.

2.4.6 MC modeling with GMMC

The specific purpose MC code GMMC was benchmarked with the experimental and simulated (MCNP5 and PENELOPE) data presented in section 2.3 and paper 1. The problem geometry was the same as in the MCNP5 and PENELOPE models of the GM counter (see figure 2.4).

The MC code GMMC was compiled using Intel Fortran compiler version 11.1. GMMC simulations were run on the CEAR cluster which is made up of 41 computing nodes. Most of these are 32-bit machines whereas a few of them are 64-bit machines with AMD Phenom 9950 Quad-core processors at 2.6 GHz [61]. Only the 64-bit machines were used while running GMMC simulations in parallel. A total of 2.5×10^5 primary photon histories were simulated (see appendix 4 for an example of GMMC input file) and due to the computational inefficiency of detailed charged particle transport, a single run on three 64-bit machines (a total of 12 cores) took about 5.5 hrs. These numbers give a picture of how time consuming the single scatter approach would be if simulations had to be run on a single PC.

The results from MCNP5, PENELOPE and GMMC as well as experimental stopping efficiency values are given in figure 2.9.

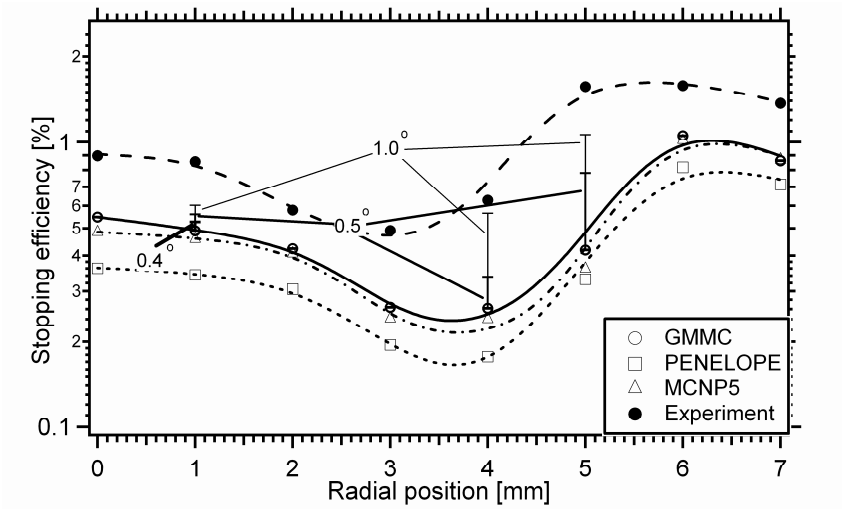

Figure 2.9 **GMMC (open circular legends and the solid best fit curve), MCNP5 (open triangle legends and the dash-dotted best fit curve), PENELOPE (open square legends and the dotted best fit curve) and experimental (solid legend and the dashed best fit curve) stopping efficiencies of the ZP1200 counter as a function of the radial position of the 3.0 mm diameter photon beam. The error bars shown on the GMMC simulated results show the effects of tilting the beam toward the cathode wall of the counter at r = 5 and 6 mm, and toward the anode tip bead at r = 1 mm.**

As described in paper 2, a chi-square analysis was conducted and it was found that the GMMC code employing detailed electron transport minimizes the reduced chi-square value when compared to MCNP5 and PENELOPE simulated stopping efficiency curves. The reduced chi-square values are shown in table 2.1.

Table 2.1 **The reduced chi-square values obtained using GMMC, MNCP5 and PENELOPE.**

MC code	χ^2_ν
GMMC	57.4
MCNP5	65.2
PENELOPE	90.04

To take into account the surface porosity of the Cr coating, the use of Cr density multiplication factor was considered also in GMMC simulations of the ZP1200 counter. However, the mismatch between the simulated and experimental curves shown in figure 2.9 as well as the simulation results that show extreme sensitivity to detector/beam misalignment shown in the same figure indicate the need for new experimental stopping efficiency data for determining a suitable density multiplication factor. For this purpose, new experiments using an uncollimated beam and detector were conducted. This time, however, the reference measurements were carried out using a 2 in. x 2 in. NaI(Tl) scintillation detector. The idea behind using no collimation was to reduce the geometric sensitivity of the GM counter to its positioning with respect to the incoming photon beam. In this case, a 10 μCi ^{241}Am disk source was used. It was placed at a sufficiently large distance to minimize the effects of the source geometry. The details of the read-out electronics and the experimental procedures can be found in paper 2.

Using the above mentioned uncollimated beam and detector geometry, an experimental gamma-ray stopping efficiency of 1.3554% was obtained. GMMC simulations were repeated using various density multiplication factors. A straight line was fitted to the simulated stopping efficiency data in order to obtain a relation between the density multiplication factor and the integrated number of counts in the GM detector. This is shown below in figure 2.10.

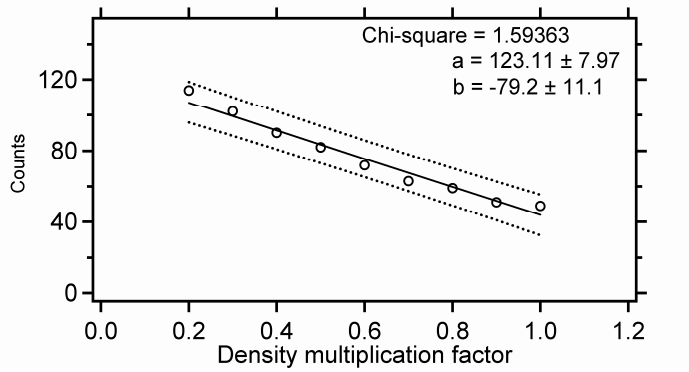

Figure 2.10 **The figure is showing a scatter plot reflecting the relation between the Cr density multiplication factor and the simulated number of counts in the GM counter. The straight line fitted to these data is shown together with the prediction band with 95% confidence interval. Also given are the chi-square value of the fit and the fitting coefficients ± one standard deviation.**

Based on the experimental results and the linear fit to the simulated data, a density multiplication factor of 0.23 was obtained.

Additionally, the experiments described in paper 1 and section 2.3 (see figure 2.4) were repeated with a rather simpler setup to address the positioning and repeatability issues. The measurement setup and read-out electronics are explained in detail in paper 2. Also, using the above mentioned Cr density multiplication factor, a final numerical experiment was carried out using GMMC.

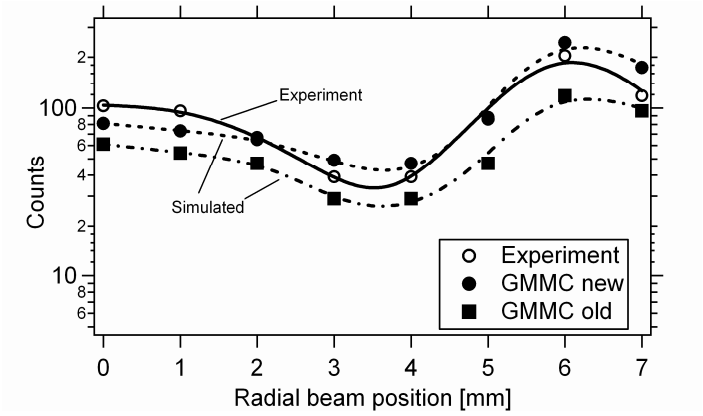

Figure 2.11 **Simulated and experimental stopping efficiencies as a function of the radial position of the 3.0 mm diameter photon beam. GMMC old: GMMC results obtained prior to the utilization of the density multiplication factor. GMMC new: GMMC results obtained utilizing the density multiplication factor in order to take into account the surface porosity of the inner Cr coating.**

The results obtained using GMMC in conjunction with a Cr density multiplication factor are presented in figure 2.11. The comparison between simulated and experimental results was again based on a chi-square test of distributions. It was seen that a reduced chi-square value of 7.0 was obtained which is an improvement by a factor of 6.0 compared to the results of paper 1. As concluded in paper 2, a reduced chi-square value of 7.0 indicates a better match between simulated and experimental stopping efficiency curves.

2.5 Enhancement of gamma-ray stopping efficiency in GM counters

As mentioned earlier in the introduction section of this thesis as well as in section 2.1, the possible utilization of GM counters in the DMD approach for subsea produced water characterization would, to some extent, depend on the identification of a method whereby the poor gamma-ray intrinsic stopping efficiency of these detectors could be improved. Therefore, the main focus in this section is on MC investigation of a method for this purpose using the validated MC model of the ZP1200 counter which is described in the previous section and paper 2. The details of the MC calculations and the subsequent analyses carried out in the study presented in this section can be found in paper 5.

2.5.1 Method of enhancing the gamma-ray efficiency

The considered method consisted of placing non-conducting disks between the anode wire and the cathode walls of the counter. The idea behind investigating the feasibility of this method is based on the fact that the fill gas of the ZP1200 counter is kept at a relatively low pressure, about 135 mbar [1], to enable gas multiplication at lower bias voltages. This means that the probability for the incident photons to cause a direct ionization in the fill gas region will be negligibly small. On the other hand, introducing a higher density and atomic number material on the path of the photons, such as the above mentioned non-conducting disks, would increase their interaction probability and lead to production of several more secondary electrons that may penetrate into the fill gas and cause a Geiger discharge.

2.5.2 Disk material

As explained in paper 5, several disk materials were considered for this purpose. The selection criterion was based on a simple calculation where the ratios between the total photon mass attenuation coefficient at 59.5 keV and the total electron stopping power at the same energy in each potential disk material were compared. Material with the highest ratio was then selected as the disk material. The results of this analysis as well as the potential disk materials considered in this work are given in table 2.2.

Table 2.2 Mass attenuation coefficients and the total electron stopping powers (at 59.5 keV) of the non-conducting disk materials considered in this work. Also given are the ratios, μ/-(dE/dx). The data are obtained from NIST XCOM and ESTAR databases [62, 63].

Disk material	Mass attenuation coefficient at 59.5 keV [cm^2/g]	Total electron stopping power at 59.5 keV [MeV cm^2/g]	Ratio [MeV^{-1}]
Silicon	0.321	4.57	0.0702
Mica	0.331	4.66	0.0710
Al_2O_3	0.237	4.64	0.0511
Teflon	0.188	4.78	0.0393
Polypropylene	0.197	6.21	0.0317
HfO_2	2.93	3.11	0.942

It is clear from the results presented in table 2.2 that HfO_2 (hafnium oxide) gives the highest ratio. This is a clear indication of the fact that HfO_2 would be the most efficient material in converting the incoming photons to secondary electrons that could penetrate into the fill gas and thereby, increase the efficiency. Therefore, it was decided to carry out MC simulations to study the feasibility of introducing HfO_2 disks inside the ZP1200 counter. A detailed discussion on the choice of optimal disk thickness is given in paper 5. Here, it will be sufficient to state that the optimal HfO_2 disk thickness was determined to be about 10 μm as this is very close to the CSDA range of electrons in this material (which is about 11 μm).

2.5.3 Simulation geometry and constraints

A sketch of the problem geometry is given in figure 2.12.

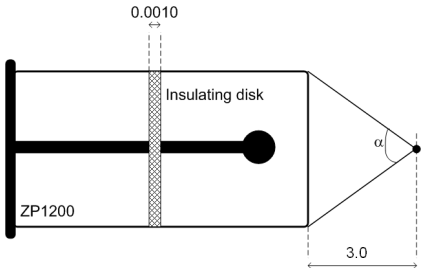

Figure 2.12 The current simulation geometry is shown. The ZP1200 counter is modified through the inclusion of a thin (thickness of 10 μm) hafnium oxide disk. α = 28.07°. All dimensions are given in cm.

As pointed out in paper 5, an important issue is the simulation of electron transport within the fill gas region. In the course of development of a validated MC model of the ZP1200 counter, a "binary" GM counter case was always assumed (see papers 1 and 2). This is, however, no longer valid in the current study as a certain fraction of electrons in the fill gas may, depending on their spatial distribution, be fully absorbed in the disk material without causing ionization or excitation of the fill gas atoms. Naturally, this effect would be more pronounced when several disks are placed inside the detector. Therefore, in the MC simulations of the new concept GM counter, the constraints were made slightly stricter by requiring that every secondary electron in the fill gas undergo an inelastic collision in the fill gas prior to incrementing particle counters. This approach requires, however, taking into account also the effects of the electric field on the transport of secondary electrons in the fill gas.

2.5.4 Analysis of the static electric field

As discussed in paper 5, the COMSOL Multiphysics simulation package [64] was used to analyze the static field inside the counter. Using COMSOL Multiphysics a model of the ZP1200 was developed. This was done using the "electric currents" interface of the COMSOL Multiphysics AC-DC module. This interface also allows the definition of thin structures by using the internal boundary condition "electric shielding". This boundary condition was used to model the inner Cr coating with thickness of about 5-8 μm that is plated onto the inner surfaces of the cathode walls as well as the thin (thickness of 10μm) insulating disk placed inside the counter. The other relevant boundary conditions were as follows: the potential at the conducting anode wire was set equal to 500 V (this is the operating voltage of ZP1200 counters recommended by the manufacturer) and the outer surface of the conducting cathode

walls was at ground potential. Simulations were run for a bare, unmodified ZP1200 and one that was modified by the introduction of a thin, insulating HfO_2 disk. In these simulations, a relatively finer mesh, i.e. a total of 127194 tetrahedral elements, was used and the total mesh volume was 7.214 cm^3. The results of the two simulations were compared with each other. As a result, it was observed that insertion of a thin non-conducting disk inside the counter does not lead to any appreciable effects on the field lines or the intensity of the radial static electric field in the vicinity of the disk (see paper 5).

2.5.5 Simulation procedure

A major limitation of GMMC is that it is not yet able to simulate charged particle transport in electromagnetic fields. An implementation of this for the purpose of simulating the first few collisions of a secondary electron in the fill gas would not be necessary as the simulation of charged particles in electromagnetic fields is already incorporated into the general purpose MC code PENELOPE. So, GMMC was instead used to generate a phasespace distribution of secondary electrons penetrating into the fill gas from the solid structures. Then, PENELOPE was used to track the path of these electrons in the fill gas taking into account also the radial electric field. This is because the simulation of secondary electrons need not be as accurate and detailed as in the solid parts of the counter. The simulation of secondary electrons in the fill gas was then terminated upon occurrence of an inelastic scattering event, and a count was registered. The entire calculation procedure is given using a block diagram representation in figure 2.13.

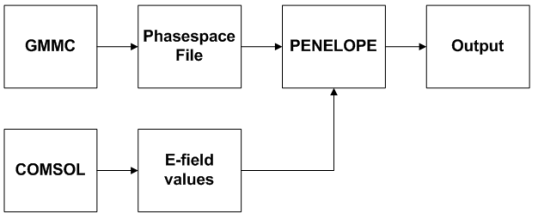

Figure 2.13 Block diagram showing the computational tools utilized in this study as well as the work flow. GMMC was used to generate a phasespace file for the secondary electrons penetrating into the fill gas whereas COMSOL Multiphysics was used to calculate the initial electric field values near the surfaces of anode rod and the anode tip bead. The output from GMMC and COMSOL Multiphysics were fed into the PENELOPE model. PENELOPE was then used to calculate the effective increase in the intrinsic gamma-ray stopping efficiency of the ZP1200 GM counter.

2.5.6 Simulation results

The initial MC simulations were carried out where a single, thin (thickness of 10 μm) HfO_2 disk was placed inside the counter. The results are given in figure 2.14.

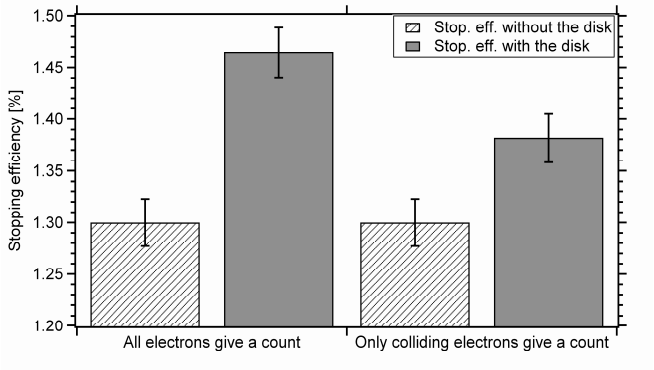

Figure 2.14 **The intrinsic gamma-ray stopping efficiency of the original and modified ZP1200 counters at 59.5 keV. The figure also shows that the effective increase in the intrinsic stopping efficiency will be somewhat lower due to loss of electrons through absorption in the solid parts of the modified ZP1200 counter.**

The results presented in figure 2.14 show that the stricter constraint summarized in this section and discussed in detail in paper 5 leads to the fact that the effective increase in the intrinsic gamma-ray stopping efficiency of the ZP1200 counter will be somewhat lower. This can be explained by a loss in the number of electrons suffering inelastic collisions in the fill gas through absorption in the solid parts of the counter. It is also clear from figure 2.14 that the introduction of a single disk will only lead to a marginal increase in the intrinsic gamma-ray stopping efficiency of the ZP1200 GM counter. The next step in this study involved, therefore, an investigation of the possibility of increasing the total number of disks inside the counter. Nonetheless, it soon became evident that the total number of disks that can be placed inside the GM counter is limited by the minimum allowable spacing between each disk. At the energy of interest, electrons have inelastic mean free path of about 0.21 cm in the fill gas [36]. This suggests that the distance between each disk should be of the order of 0.20 cm in order to minimize electron losses.

The results of the MC simulations, in which the total number of disks was increased gradually from 1 to 15, are presented in figure 2.15.

As can be seen in figure 2.15, introducing more disks inside the counter, in fact, leads to an appreciable increase in the intrinsic gamma-ray stopping efficiency. The MC simulations predict approximately a threefold increase in the stopping efficiency when a total of 15 disks are placed inside the detector. Nevertheless, it can also be seen that the electron loss through absorption in the solid parts prior to suffering inelastic collisions in the fill gas becomes even more pronounced as the number of disks is increased.

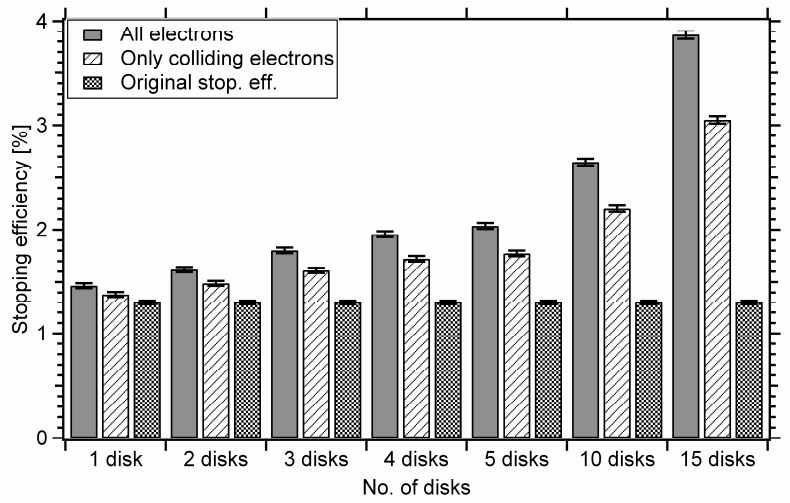

Figure 2.15 **Intrinsic gamma-ray stopping efficiency of the ZP1200 counter, at 59.5 keV, as a function of the total number of insulating disks; given for the case in which all secondary electrons in the fill gas are counted, and for the case in which only secondary electrons that suffer an inelastic collision in the fill gas are counted. Also given is the stopping efficiency of the unmodified, original ZP1200 GM counter.**

3. PGNAA for produced water characterization

As explained in chapter 1 of this thesis, the DMD measurement principle alone cannot be used to provide detailed analyses of subsea produced water samples as this would require a full compositional/elemental analysis of the pertinent produced water sample. On the other hand, PGNAA is a well-known non-destructive, non-intrusive and on-line elemental/compositional analysis method for bulk samples which found a variety of applications within the industry and other fields such as analysis of coal and food [21-24], detection of explosives [65] and other illicit materials [66]. Therefore, in this work, the feasibility of applying the PGNAA method to characterization of produced water samples is investigated. In the following section, section 3.1, a brief background of the PGNAA project will be given. This will be followed by a brief description of the physical processes involved in the PGNAA method. Also, a brief description of the MCLLS approach will be given as this is the quantitative analysis technique utilized in this work. A subsection will be devoted to one of the major contributions of this thesis which improves the sensitivity of the MCLLS approach and to some extent provides an adequate treatment of one of the major limitations of the MCLLS approach, i.e. the ill-conditioning in the MCLLS approach. Finally, the main results of the experimental feasibility studies will be presented. The experimental work was carried out by the author during a research stay at the North Carolina State University, USA during fall 2010 and spring 2011. Detailed discussions and descriptions of the experimental work as well as MC simulations and the proposed improvement of the MCLLS approach can be found in papers 3 and 4.

3.1 Background of the PGNAA project

The major drawback of the DMD measurements based on measurements of transmitted and scattered gamma-rays from the sample of interest is that it will not provide any useful information on the elemental composition of the sample. In analyses of produced water samples, the chemical composition of the sample of interest can only be estimated through combination of DMD measurements and several other measurement modalities such as ultrasound measurements and electrical conductivity measurements [10].

It has previously been demonstrated through experiments and MC simulations that the DMD measurements will provide excellent sensitivity to the salinity of produced water samples [10, 11, 13, 17].

In these previous efforts studying the feasibility of the DMD measurement approach to characterize produced water samples, four different salt types were used to prepare several salt/water solutions. These are shown in table 3.1.

Table 3.1 Salt/water solutions used in the previous feasibility studies with the DMD measurement principle [13].

Salt	Weight percent of salt in water (%)					
NaCl	2	4	6	10	14	18
$MgCl_2$	2	4	6	10		
$CaCl_2$	2	4	6	10		
$SrCl_2$	1	2	3	4		

The salt/water solutions given in table 3.1 were then used in the experimental and MC studies of the DMD principle. For clarity, some of the earlier results with the DMD measurement principle are also given here in figures 3.1 and 3.2. Figure 3.1 shows the results of measurements of 59.5 keV gamma-rays transmitted through 48.4 mm of salt/water solutions given in table 3.1 whereas figure 3.2 shows those obtained for scattered gamma-rays [13]. The reader is referred to figure 2.2 for an overview of the DMD measurement principle.

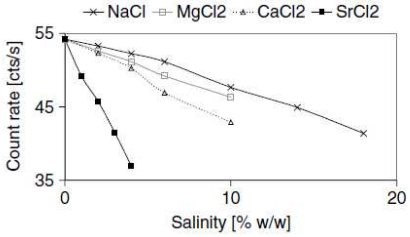

Figure 3.1 Measurements of radiation transmitted through 48.4 mm of salt/water solutions (see figure 2.2 for an overview) as a function of salinity and salt type. See ref. [13] for details of the measurement setup[3].

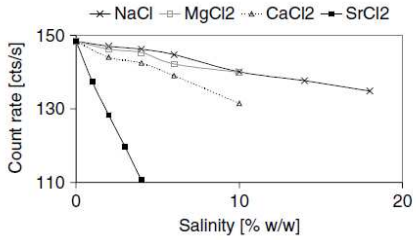

Figure 3.2 Measurements of scattered radiation from salt/water solutions (see figure 2.2 for an overview) as a function of salinity and salt type. See ref. [13] for details of the measurement setup[3].

In this thesis, there will be no elaborate discussions on the results of the DMD measurements as these can be found in [10, 11, 13, 17]. It is sufficient to state that, as can be seen in figures 3.1 and 3.2, the measurements of transmitted and scattered 59.5 keV gamma-rays will provide useful information on the salinity and type of salt in various produced water samples containing single salts. However, the DMD measurements alone cannot be used to identify and characterize uniquely the produced water samples that contain arbitrary mixtures of different salts unless a combination of different measurement modalities is considered [10]. Moreover, the DMD measurements alone cannot be used to identify chemical process additives such as Mono-Ethylene-Glycol (MEG) and other substances [10] that may be found in arbitrary produced water samples in addition to various salt types. In cases where such information is required, the DMD measurements must be used in conjunction with other measurement modalities. Otherwise, use of other, more sensitive techniques must be considered.

In the work presented in this chapter, the use of PGNAA method in conjunction with the MCLLS approach for the subsequent quantitative analysis is proposed as an alternative to the currently pursued DMD approach. In fact, the feasibility of utilizing PGNAA in conjunction with the MCLLS approach was recently examined in the context of a subsea multiphase flow

[3] Figures are reproduced with permission from the publisher (IOP Publishing Ltd.).

measurement problem using MC simulations [5]. Results obtained in this previous work by Wang et. al. [5] indicated that PGNAA in conjunction with the MCLLS approach would be feasible for determining the respective amounts of gas, oil, water and salt in arbitrary multiphase mixtures. This recent development has also prompted consideration of the use of the PGNAA method for detailed characterization of produced water samples.

One of the main contributions of this thesis is an experimental feasibility study investigating the applicability of the PGNAA method in conjunction with the MCLLS approach for characterization of produced water samples. The results of this feasibility study are discussed in detail in paper 3, and briefly presented in section 3.4. In the next two sections, section 3.2 and section 3.3, an overview of the PGNAA method as well as a brief introduction to the MCLLS approach for the quantitative analysis will be given.

3.2 An overview of the PGNAA method

As the PGNAA method is considered as an alternative to the DMD measurements for characterization of produced water samples, a short introduction to the pertinent physics involved in PGNAA is in order. It should, however, be mentioned that giving an elaborate introduction to the physics of neutron transport through absorbers would be out of the scope of this work. Instead, the focus here is on the neutron-matter interaction mechanisms that have substantial relevance for the signal generation in the PGNAA method. The interested reader can refer to [59, 67] for more elaborate discussions on neutron interactions.

The PGNAA method is based on bombarding a sample of interest with thermal or fast neutrons. Neutrons, being uncharged like photons but with a finite mass, are not affected by the Coulomb field of the nucleus and therefore interact directly with the nucleus of an atom rather than the electron cloud surrounding it. Also, as neutrons interact with matter relatively infrequently, they may penetrate into much greater depths in the absorber than energetic charged particles. There are two important neutron-matter interaction mechanisms that contribute to the overall signal in PGNAA. One of these is the neutron inelastic scattering event, i.e. (n,n`γ) reaction. In an inelastic scattering event, the incoming neutron will lose some of its initial energy and change its direction of propagation. During this process, some of the kinetic energy transferred from the incident neutron to the target nucleus is spent to place the target nucleus into an excited state. The average energy loss will, in inelastic scattering events, depend on the energy levels within the nucleus [67]. If the energy levels of the excited states are too high compared with the pre-collision energy of the incident neutron, inelastic scattering cannot take place. Therefore, the inelastic scattering of neutrons from target nuclei is referred to as a threshold reaction.

Table 3.2 The neutron inelastic scattering threshold energies of some nuclei which are pertinent to the current project [68].

Nucleus	Threshold Energy [keV]
O-16	6049.4
Na-23	440.4
Cl-35	1219.4
Cl-37	1726.6
Sr-86	1080.0
Sr-87	388.0
Sr-88	1840.0

The inelastic scattering threshold energies for some nuclei relevant to this work are given in table 3.2. In particular, the hydrogen nucleus which is highly abundant in produced water samples does not have any excited states. Therefore, in this case, the probability of an inelastic scattering event to take place is zero. Upon suffering an inelastic scattering event, the de-excitation of the excited nucleus can take place through emission of prompt gamma-rays or internal conversion where the excess energy is transferred to an extra-nuclear electron which is then ejected from the atom. This process can be followed by the emission of characteristic X-rays [21]. The energy loss caused by the inelastic scattering of an incident neutron from a target nucleus can be formulated as follows [67]:

$$E_{out} = \left(\frac{A}{A+1}\right)^2 \left[E_{in} - \frac{Q(A+1)}{A}\right] \tag{3.1}$$

where E_{out} is the energy of the outgoing neutron, E_{in} is the energy of the incident neutron, A is the atomic weight of the target nucleus and Q is a value that should equal the energy of the excited level of the nucleus.

The second neutron-matter interaction mechanism that contributes the most to the prompt gamma-ray production is the absorption of slowed down or thermal neutrons by the nuclei, i.e. the thermal neutron capture, (n,γ), event.

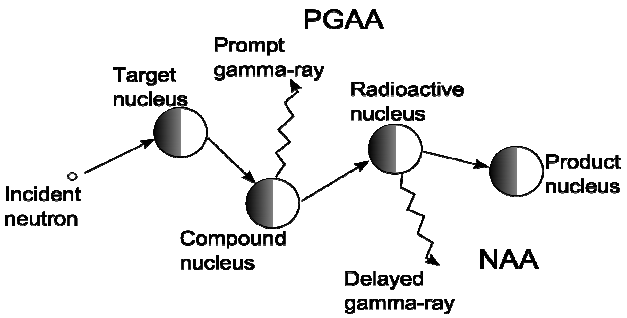

Figure 3.3 **A schematic overview of the thermal neutron capture reaction. The target nucleus absorbs the incident neutron and thus, a highly unstable compound nucleus is formed. The compound nucleus de-excites promptly by emitting few high energy gamma-rays. Measuring these prompt gamma-rays is the basis of the PGNAA method. In some cases, the daughter nucleus may remain in an excited state. In these cases, the daughter nucleus will de-excite to form the product nucleus by the emission of the so-called delayed gamma-rays with a given half-life. Measuring only these delayed gamma-rays is the basis of the more conventional neutron activation analysis (NAA).**

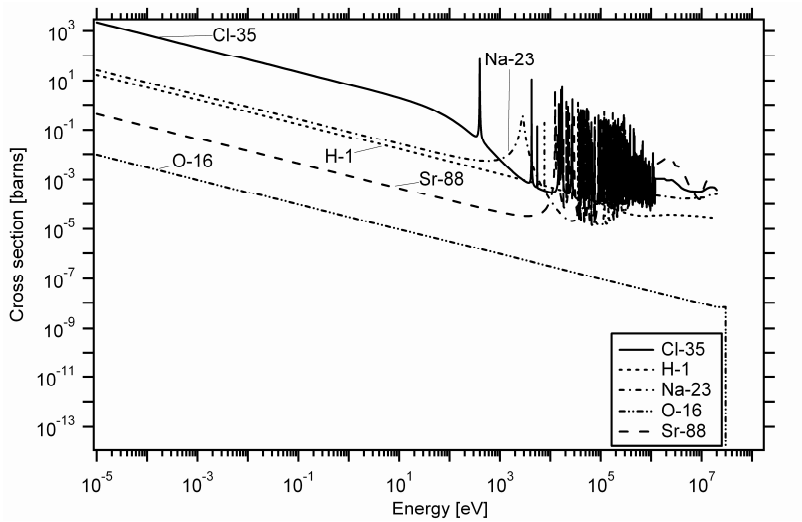

Figure 3.4 **Neutron capture cross sections of Cl-35, H-1, Na-23, O-16 and Sr-88 [68]. Cl-37, Sr-86 and Sr-87 are omitted as these have relatively low isotopic abundances.**

This interaction mechanism will have enhanced probability of taking place when energetic or fast neutrons (with energy of the order of few MeV) in the sample are slowed down to thermal energies (with energy of the order of 0.025 eV) after suffering a sufficient number of elastic and inelastic scattering events. A highly unstable compound nucleus is formed when the incident neutron is absorbed by the target nucleus. The compound nucleus will then de-excite back to its ground state through the emission of prompt gamma-rays. These gamma-rays are referred to as prompt since the decay time, which is of the order of 10^{-9}-10^{-12} s, following the neutron capture reaction is much shorter than the resolving time of the detection system. A schematic overview of the neutron capture reaction is shown in figure 3.3. Also, neutron capture cross-sections of few elements that are relevant to the work presented in this thesis are given in figure 3.4.

As can be seen in figure 3.3, in some cases the unstable compound nucleus may, upon emitting energetic prompt gamma-rays, form a daughter nucleus that remains in an excited state. The daughter nucleus will then de-excite into its ground state to form the stable product nucleus by emitting so-called delayed gamma-rays with a given half-life. Monitoring these delayed gamma-rays is the basis of the more conventional neutron activation analysis (NAA). The application of the NAA method for characterization of produced water samples was not considered as the intensities of the delayed gamma-rays will, in many cases, be much weaker than the intensities of prompt gamma-rays. This would lead to relatively longer measurement times in order to achieve good SNR values. Another disadvantage of NAA would be in that, immediately after the irradiation of the sample under investigation, removal of the neutron source would be needed in cases where radioisotopic neutron generators such as Cf-252 and Americium-Beryllium (AmBe), are utilized. This would make the design of a potential analyzer based on NAA more complicated and less robust as moving parts would be required.

Common to both interaction mechanisms described above, i.e. the neutron inelastic scattering and thermal neutron capture reactions, is the fact that both result in production of energetic prompt gamma-rays that are characteristic of every element and of every isotope of every element. Monitoring the energies of these gamma-rays that are unique to a given element or to

a given isotope of a given element, with a suitable gamma-ray spectrometer enables elemental/isotopic analysis using PGNAA. In figure 3.5, a sketch providing an overview of a typical, transmission mode industrial radioisotope gauge based on the PGNAA method is given. Figure 3.5 provides also a simplified block diagram of the associated read-out electronics in applications of the PGNAA method.

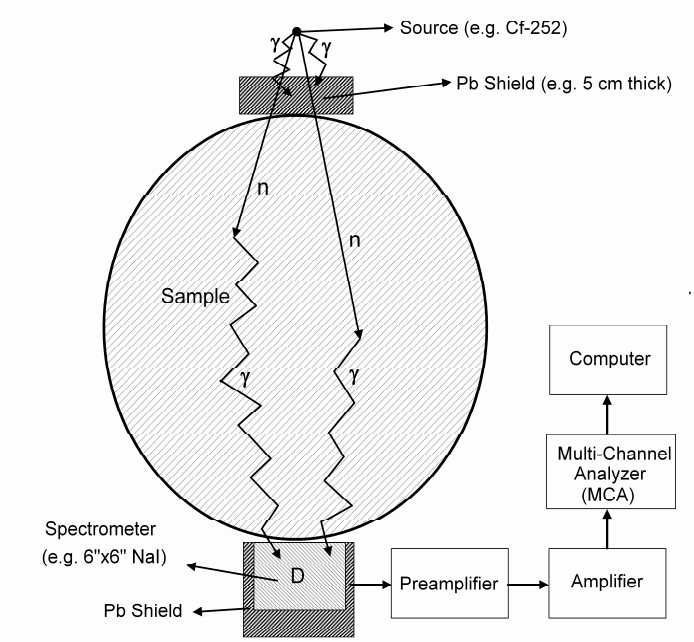

Figure 3.5 **A sketch showing an overview of the PGNAA method as well as a simplified block diagram of the read-out electronics. In cases where radioisotopic Cf-252 neutron sources are utilized, a relatively thick lead shield can be placed between the source and the sample to attenuate the energetic fission gamma-rays emitted from a Cf-252 source. Large detectors, such as 6 in. x 6 in. NaI scintillators, can be utilized in order to increase the overall efficiency of the measurement gauge.**

A MC simulated PGNAA spectrum of a salt/water solution containing 2% NaCl and 98% H_2O is given in figure 3.6. The spectrum is obtained by exposing the solution to Cf-252 spontaneous fission neutron source and monitoring the energies of the resulting prompt gamma-rays with a 6 in. x 6 in. NaI(Tl) scintillation detector. The counts in each channel of the spectrum are normalized to be per starting neutron history.

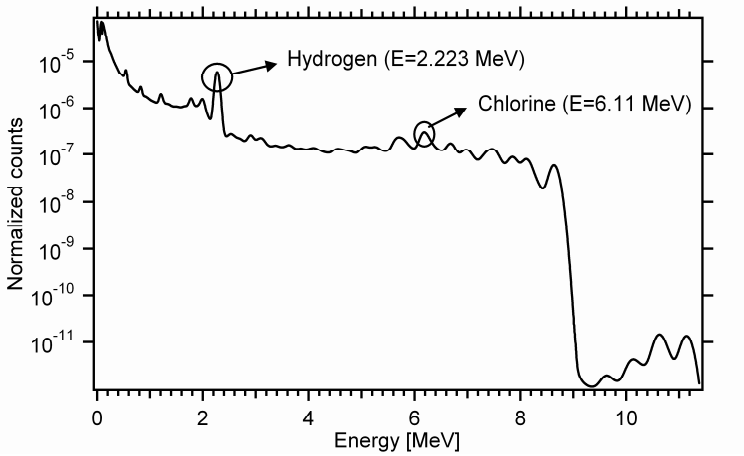

Figure 3.6 Prompt gamma-ray spectrum of a salt/water solution containing 2% NaCl and 98% H_2O obtained through MC simulations. The solution is exposed to a Cf-252 spontaneous fission neutron source whereas a 6 in. x 6in. NaI(Tl) scintillation detector was used to monitor the resulting prompt gamma-rays. The counts in each channel are normalized to be per history.

In addition, due to the fact that neutrons interact with the absorber relatively infrequently and thus, penetrate into great depths in the absorber; that no sample preparation is needed; and that chemical composition of the sample is not altered, the PGNAA method is said to offer a very rapid, on-line and non-destructive elemental analysis of bulk samples.

3.3 Introduction to the MCLLS approach for quantitative analysis

In PGNAA, the characteristic prompt gamma-rays emitted from the nuclei are monitored using a gamma-ray spectrometer such as NaI(Tl) scintillation or high-purity Ge semi-conductor detectors. The sample of interest is exposed to thermal or fast neutrons and the resulting gamma-ray spectrum is examined. The examination of the gamma-ray spectrum implies identifying the photopeaks in the spectrum. The energies of these photopeaks would then reveal which elements are present in the sample. This is essentially the basis of the so-called single peak analysis [21]. The identification of photopeaks and thereby the corresponding elements is carried out by comparing the acquired spectrum with known prompt gamma-ray data. Typically, the most intense peaks in the spectra are exploited and the mass fraction of a certain element is calculated based on the integral number of counts in the corresponding photopeaks. A more detailed treatment of the single peak analysis can be found in [21]. The most important downside of the single peak analysis is the fact that the rest of the spectrum, i.e. the Compton continua, is considered to be background and is disregarded. The single peak analysis is by far the most commonly utilized quantitative analysis approach in applications of PGNAA [21]. However, there exist significant challenges in the implementation of the inverse analysis through the single peak method. In many cases, the acquired spectrum will be extremely complex. For example, a constituent of a sample being investigated may have an extremely high thermal neutron capture cross section. This may in turn cause a significant distortion in the acquired spectrum through neutron self-shielding [21]. In addition, as prompt gamma-ray spectra of most samples will contain thousands of gamma-lines, there is a substantial probability that spectral interference will constitute a major source of error in the quantitative analysis [21]. The distortion introduced through spectral interference will, on the other hand, depend on the gamma-ray spectrometer used to

record the final spectrum. It is now a common knowledge that, in many permanently installed industrial gauges based on the PGNAA method, NaI(Tl) or BGO scintillation detectors are preferred [69, 70]. These detectors are known to have poor energy resolution [1, 19, 69]. Therefore, in cases where the prompt gamma-ray spectra are recorded using scintillation detectors, spectral interference, i.e. overlapping of photopeaks, will be unavoidable. In addition, some elements in the sample may have extremely low neutron capture cross-sections or some samples may contain only trace amounts of certain elements. In those cases, the photopeaks from these elements may not be visible in the acquired spectrum as these may be totally masked by the much higher intensity peaks from other elements and their associated Compton continua.

In the work presented in this thesis, an alternative method, the so-called library least squares (LLS) technique, instead of the above mentioned single peak analysis is utilized for the inverse quantitative analysis. The LLS technique is a well-established analysis technique that has found several applications in gamma-ray spectroscopy such as analysis of gamma-ray scintillation spectra [71]. It has also been successfully applied to PGNAA analyzers [5, 27]. The main reason for pursuing the application of the LLS technique in this work is the paper by Gardner et. al. [72] in which it was shown that the LLS technique is more sensitive and robust than the single peak analysis. The main assumption of the LLS technique is that the total count-rate in any "unknown" spectrum can be given as a linear combination of the count-rates in the individual library spectra whereas a library spectrum is the prompt gamma-ray spectrum of a single constituent of the sample. A mathematical expression of this can be given as follows:

$$R_{s,i} = \sum_{j=1}^{n} \alpha_j R_{j,i} + e_i \tag{3.2}$$

where $R_{s,i}$ is the count rate in the i^{th} channel of the unknown sample spectrum, $R_{j,i}$ is the count rate in the i^{th} channel of the j^{th} component, α_j is the multiplier of the j^{th} component and e_i is the error in the i^{th} channel.

In addition to being more sensitive than the single peak analysis, the LLS technique can be said to have the following advantages:

- Unresolved peaks are treated automatically.
- The entire prompt gamma-ray spectrum is used in the course of the calculations, i.e. both photopeaks and the associated Compton continua.
- Residuals may reveal whether or not there are missing libraries.
- Standard deviations of the mass fraction estimates are directly available from the LLS search. The calculational procedures involved in the determination of these standard deviations are presented in detail in a paper by Arinc et. al. [25].

In spite of the advantages listed above, the LLS technique does have a major limitation in that this technique requires the pertinent prompt gamma-ray libraries of each constituent to be available prior to carrying out the linear search. In addition, the LLS technique assumes a linear relation between the count-rates in the "unknown" spectrum and the count-rates in the individual library spectra. As such, the LLS technique cannot be directly applied to quantitative analysis of PGNAA spectra. This is due to the fact that the PGNAA method itself

is inherently non-linear in the sense that the contribution from the library spectrum of each constituent in the sample will depend not only on the amount of that constituent but also on the amounts of every other constituent that make up the sample of interest. Generating accurate experimental library spectra that take into account such non-linear matrix effects would be an extremely difficult, costly and time-consuming task. Therefore, the utilization of the MCLLS approach that treats these non-linear effects through generating the library spectra with accurate forward MC simulations was proposed [27]. The non-linear matrix effects are an integral part of the MC simulations and therefore, an integral part of the MC generated library spectra. Another obvious advantage of using MC simulations for generating library spectra is the elimination of the need for experimental calibration and use of standard samples. In a stepwise fashion, the MCLLS approach can be summarized as follows:

1) Obtain or otherwise assume an initial composition of the "unknown" sample.
2) Perform MC simulations to obtain the relevant library spectra of each constituent.
3) Execute a LLS search. The calculated fitting coefficients will, upon normalization, return the weight fractions of pertinent elements in the sample.
4) In case the LLS calculated amounts are so far apart from the initial estimate of the sample composition that the linearity assumption cannot be made, go back to step 2 and re-iterate MC simulations using the LLS calculated amounts as the new sample composition.

The LLS search will return the fitting coefficients through minimizing the reduced chi-square value:

$$\chi_v^2 = \sum_{i=1}^{m} \frac{e_i^2}{(m-n)\sigma_i^2} \tag{3.3}$$

where *(m-n)* is the number of degrees of freedom, e_i is the error in the i^{th} channel and σ_i is the standard deviation in the i^{th} channel. The reduced chi-square value is minimized by taking its partial derivative with respect to the library multipliers and setting the derivative equal to zero. This leads to the production of a set of simultaneous linear equations. The set of linear equations can then be solved in a least-squares fashion. In the following, a more general mathematical description of this method, which follows that of [73], is given.

Assuming an expression of the form:

$$y(x) = \sum_{k=1}^{m} a_k f_k(x) , \tag{3.4}$$

it can be concluded that there is a linear relation between the *y(x)* variables and the independent variables $f_k(x)$ for $k = 1,...,m$. Equation (3.4) describes a linear dependence and therefore, a linear least-squares search can be carried out to estimate the optimal values for the parameters $a_1,....,a_m$ that describe the dependence of *y* values on the *x* values. This is achieved by minimizing the so-called chi-square[4], χ^2, value which can be given as follows:

[4] The pertinent derivation is worked out using the chi-square, χ^2, instead of the reduced chi-square, χ_v^2.

$$\chi^2 = \sum_{i=1}^{N} \frac{1}{\sigma_i^2} \left\{ y_i - \sum_{k=1}^{m} a_k f_k(x_i) \right\}^2 , \tag{3.5}$$

where σ_i are the uncertainties (one standard deviation) of the corresponding y_i values. The minimum of χ^2 is found by setting the partial derivatives of χ^2 with respect to the parameters equal to zero. This can be formulated as follows:

$$\frac{\partial \chi^2}{\partial a_l} = -2 \sum_{i=1}^{N} \frac{1}{\sigma_i^2} f_l(x_i) \left\{ y_i - \sum_{k=1}^{m} a_k f_k(x_i) \right\} = 0 ,$$

$$\sum_{k=1}^{m} a_k \sum_{i=1}^{N} \frac{1}{\sigma_i^2} f_k(x_i) f_l(x_i) = \sum_{i=1}^{N} \frac{1}{\sigma_i^2} f_l(x_i) y_i . \tag{3.6}$$

Equation (3.6) represents a set of m linear equations which can also be given in matrix notation where a square matrix ***F*,** also referred to as the covariance matrix, and a column matrix ***H*** are defined. Then the expression (3.6) can be written as:

$$\sum_{k=1}^{m} F_{l,k} a_k = H_l , \tag{3.7}$$

or in matrix notation:

$$\mathbf{FA = H} \tag{3.8}$$

The elements of the ***F*** and ***H*** matrices can be given as follows:

$$F_{l,k} = \sum_{i=1}^{N} \frac{1}{\sigma_i^2} f_k(x_i) f_l(x_i) \tag{3.9}$$

$$H_l = \sum_{i=1}^{N} \frac{1}{\sigma_i^2} f_l(x_i) y_i . \tag{3.10}$$

The elements of the column matrix ***A***, i.e., $a_1, a_2, ..., a_m$, can be found by solving the set of linear equations given in equation (3.8). This can be done by multiplying both sides of equation (3.8) with the inverse of the square matrix ***F***:

$$\mathbf{F^{-1} FA = H F^{-1}} \tag{3.11}$$

$$\mathbf{I A = H F^{-1}} \tag{3.12}$$

where ***I*** is the so-called identity matrix. Essentially, the most critical part of these calculations is the calculation of the inverse of the covariance matrix ***F***. Different methods can be used to calculate the inverse of a matrix. Gauss-Jordan elimination is one of the techniques that are mostly commonly employed. Discussing the details of matrix inversion algorithms is out of

the scope of this thesis. However, the interested reader is referred to [73] for a more comprehensive discussion.

3.3.1 Ill-conditioning in the MCLLS approach

As discussed in section 3.3, the most critical component of a LLS search will be the inversion of the covariance matrix. A more general solution of the set of linear equations (see equation 3.8) can be given as follows:

$$\mathbf{A} = (\mathbf{F}^{\mathrm{T}}\mathbf{F})^{-1}\mathbf{F}^{\mathrm{T}}\mathbf{H} \tag{3.13}$$

It is also a well-known fact that the determinant of a matrix must be non-zero, i.e. the matrix must be non-singular, for the matrix to be invertible. In the LLS calculations, it is the covariance matrix that has to be inverted and in certain cases, the non-singularity of the covariance matrix will not provide sufficient information on the stability of the least-squares solution. The naïve least-squares technique may result in estimation of the elements of the column matrix $\boldsymbol{A}$ with relatively high uncertainties. This essentially makes the results of the naïve least-squares calculations useless. This will be the case whenever the covariance matrix is ill-conditioned [74]. As stated in paper 4, the covariance matrix $\boldsymbol{F}$ will be ill-conditioned in cases where:

- the library spectrum of a constituent is similar in shape to any of the library spectra of the other constituents in the sample or to linear combinations of these libraries, i.e. when two or more libraries are linearly correlated.
- there exists a library spectrum with negligible contribution to the total prompt gamma-ray spectrum. This may be the case whenever there are trace amounts of certain constituents or other constituents with relatively low thermal neutron capture cross-sections in the sample. The count-rates in the library with negligible contribution may then be of the order of, or less than the standard deviation in the count-rates of the total prompt gamma-ray spectrum.

The ill-conditioning of the covariance matrix will lead to highly uncertain solutions in the LLS search. This will, in turn, reduce the sensitivity of the MCLLS approach in such cases as the solutions will be very sensitive to small changes in the arguments of the matrices. Moreover, the former of the two points stated above, will be directly dependent upon the energy resolution of the spectrometer used in the measurements [69]. As stated in [69], using a spectrometer with good energy resolution will reduce the ill-conditioning of the covariance matrix. However, in many field applications, scintillation detectors are preferred due to their robustness; and the ill-conditioning of the covariance matrix will almost be entirely unavoidable when using scintillation detectors due to their poor energy resolution.

To the best of the author's knowledge, a rigorous treatment of the ill-conditioned cases in the MCLLS approach has not previously been presented. One of the major contributions of the work presented in this thesis is, therefore, providing a rigorous treatment of such ill-conditioned cases in the MCLLS approach. An adequate treatment of such cases in the MCLLS approach also has important practical implications as the common practice has been to leave out the problematic libraries in the LLS search and then to calculate the amounts of the remaining constituents [9]. In certain cases, it was also suggested to use PGNAA analyzers in combination with other measurement principles to overcome the ill-conditioning in the subsequent MCLLS calculations [5].

3.3.2 Initial considerations to treat the ill-conditioned cases

As mentioned earlier, one of the major objectives of the work presented in this thesis was to study the feasibility of applying the PGNAA method in conjunction with the MCLLS approach for produced water characterization. The main points of this work are summarized in section 3.4 whereas a detailed treatment can be found in paper 3. At the moment, it will be sufficient to state that the ill-conditioning in the MCLLS approach posed a significant challenge also in the pertinent feasibility study. In the feasibility study presented in paper 3 and section 3.4, the ill-conditioning in the MCLLS approach was treated through the implementation of an indirect method which is based on forming new libraries that are combinations of the existing library of each constituent and thereby forming new covariance matrices with much lower condition numbers. The condition number is an indicator of how well- or ill-posed a linear system is [74, 75], and it was calculated as the ratio between the largest and the smallest singular values of the covariance matrix. The singular values of the covariance matrix were calculated by performing the singular value decomposition (SVD) [75]. As a rule of thumb, a condition number of about 1.0 is considered to reflect the fact that the linear system in question is a well-posed one. Generally, the higher the condition number, the more ill-posed the linear system is. Although the details of the indirect method will not be discussed here (see paper 3), it is important to state that the indirect method has one serious limitation in the sense that it relies on identification of library combinations that minimize the condition number of the covariance matrix. As such, the amounts of single constituents are not readily available from the indirect method. This means that the amount of a certain constituent will have to be determined in a recursive manner. This, in turn, will lead to the fact that the uncertainties in the LLS estimated amounts may be somewhat high due to error propagation.

3.3.3 Proposed treatment of the ill-conditioned cases

On the other hand, in the work presented in detail in paper 4, a new iterative approach to handling ill-conditioned cases was proposed and the use of the naïve least-squares calculations as well as the previously proposed indirect method was no longer pursued. The newly proposed iterative approach is, in a similar fashion to the indirect approach described in paper 3, based on minimizing the condition number of the covariance matrix in the LLS search. The condition number of the covariance matrix was again calculated as the ratio between the largest and smallest singular values of the covariance matrix. The details of the proposed iterative approach as well as a more detailed discussion on the differences between the iterative approach and the indirect method are given in paper 4. However, for the sake of completeness, the proposed iterative approach to treat ill-conditioned cases in the MCLLS calculations can be given as follows:

1) For each constituent, construct two libraries where one library is a single constituent and the other is the sum of the rest of the constituents.
2) For each case, examine the condition number of the covariance matrix.
3) Choose the fit that yields the lowest condition number.
4) Repeat steps 1) - 3) against the residual obtained from the best fit that yielded the lowest condition number and remove the library of the single constituent.

As can be seen, the most significant advantage of the iterative approach over the indirect method is the fact that the amount of a single constituent will be readily available at the end of

a single iteration. As discussed in paper 4, this would also make the potential implementation of the new iterative approach in a field application much more practical and less cumbersome when the total number of libraries increases.

The proposed iterative approach was tested in a multiphase flow problem previously treated by Wang et. al. [5]. This was identified to be a particularly difficult problem as all phase libraries with the exception of the salt and background libraries will be highly correlated due to the fact that both oil, gas and water libraries will be dominated by the contributions from hydrogen. In addition, the oil and gas libraries will exhibit the same spectral shape as both contain varying amounts of carbon and hydrogen elements. Under these circumstances, the covariance matrix will be strongly ill-conditioned. In the work by Wang et. al., the proposed approach to overcome the ill-conditioning in the MCLLS approach consisted of combining a PGNAA analyzer with a traditional gamma-ray densitometer. However, if a method to treat the ill-conditioning in the MCLLS approach could be identified, the PGNAA analyzer alone could be sufficiently sensitive to provide the separate phase amounts in a multiphase flow. Due to this potential practical consequence, the hydrocarbon multiphase flow problem was selected as an example to demonstrate the feasibility of the proposed iterative approach. A thorough discussion of the calculations involved in the determination of the separate amounts of gas, oil, water and salt phases in a hydrocarbon multiphase flow problem is given in paper 4. Here it will be sufficient to mention that the results presented in paper 4 show that the proposed iterative approach suppresses the ill-conditioning in the multiphase flow problem significantly and enables much more accurate calculations of the separate phase amounts.

3.4 PGNAA in conjunction with the MCLLS approach for produced water characterization

To demonstrate the feasibility of the PGNAA method in conjunction with the MCLLS approach for produced water characterization, an experimental study was conducted by the author during a research stay at the Center for Engineering Applications of Radioisotopes (CEAR) at North Carolina State University during fall 2010 and spring 2011. In this section, only the most relevant steps and results of the feasibility study will be given. A more detailed discussion can be found in paper 3.

At this initial stage, the design of the PGNAA analyzer was kept as simple as possible without considering the specific geometry of the SOFA prototype shown in figure 1.3. This was done so as to simplify the subsequent MC modeling of the analyzer.

3.4.1 Neutron source

In the experimental feasibility work, a 1 μg Cf-252 spontaneous fission neutron source was used. In spite of its relatively short half-life the Cf-252 spontaneous fission neutron source is frequently applied in applications that require compact, portable and cost-effective neutron sources. Some examples of these applications are the PGNAA for on-line process monitoring [21, 22], detection of explosives and other illicit materials [65, 66] and oil well logging [9]. Some of the most pertinent properties of the Cf-252 neutron source are given in table 3.3.

Table 3.3 **Some properties of the Cf-252 spontaneous fission neutron source [19].**

Neutron yield	2.34×10^{12} n s^{-1} g^{-1}
Neutrons per fission	3.8
Average neutron energy	2.14 MeV
Half-life	2.65 years

The Cf-252 source will emit neutrons with an associated energy distribution which can be approximated by a Maxwellian distribution [67]. As can be seen in figure 3.7, the spectrum is proportional to square root of the energy at low energies and decreases exponentially at high energies. In many cases, it would be necessary to moderate these energetic neutrons. However, use of moderators was not considered in this work due to the high abundance of light elements such as hydrogen in produced water samples.

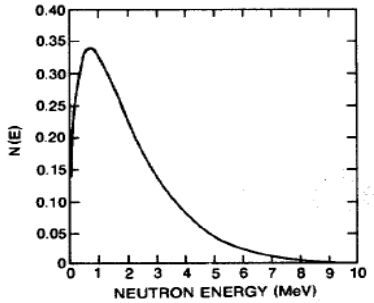

Figure 3.7 **Energy distribution of neutrons from a Cf-252 spontaneous fission neutron source as approximated by a Maxwellian distribution [67].**

3.4.2 Measurement geometry

In addition, the neutrons emitted from a Cf-252 source will be accompanied by the emission of highly energetic spontaneous fission gamma-rays [67]. It is important to ensure attenuation of these gamma-rays in order to avoid excessive dead-time in the gamma-ray spectrometer as well as to minimize the contribution from these gamma-rays to the overall background in the measurements. In the experimental setup this was achieved by placing the 1 μg Cf-252 source in a 4.5 cm thick lead container and by shielding the sample from the source by using a 5.1 cm thick lead block as shown in figure 3.8. Also, in order to reduce the dead-time further, the source to sample separation was kept at about 39.4 cm.

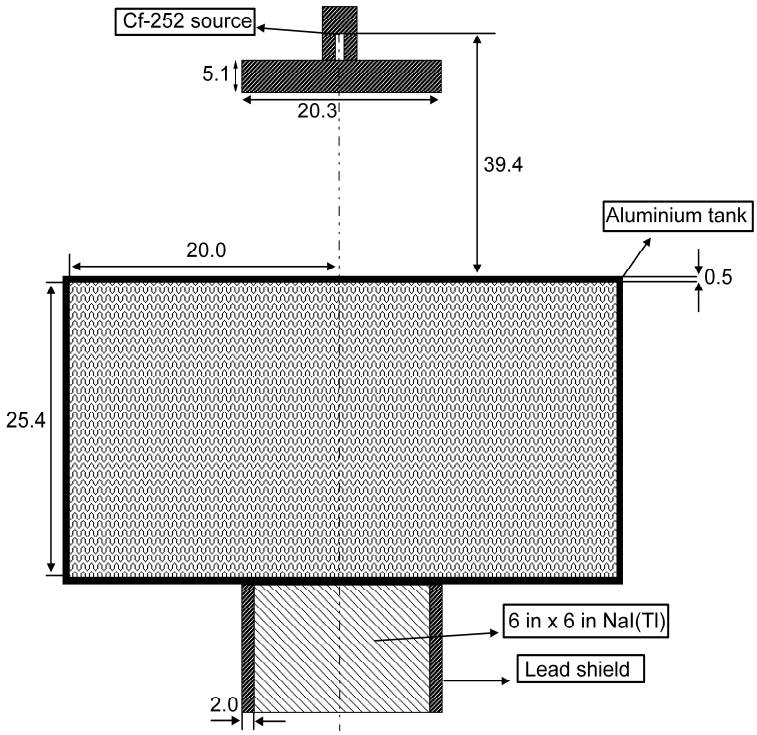

Figure 3.8 **A sketch of the experimental and simulation geometry used in this feasibility study. All dimensions in the figure are given in units of cm.**

Moreover, in analyzers based on PGNAA, the sample container should ideally be made up of materials that neither scatter nor absorb the incident neutrons [21]. For this purpose, it was decided to use aluminum (Al) as the sample container material. The pertinent dimensions of the Al container are shown in figure 3.8.

An important component of the experimental system, which is omitted in figure 3.8, is the concrete wall that was built around the entire experimental system. This had critical importance as to reduce the neutron and gamma doses to the surroundings and laboratory workers to an acceptable level.

3.4.3 Gamma-ray spectrometer

As can be seen in figure 3.8, in spite of its relatively poor energy resolution, the monitoring of the prompt gamma-rays was achieved using a large, 6 in. x 6 in. NaI(Tl) scintillation detector. It was thought that NaI detectors would also help make the final design of the analyzer more robust than an analyzer that employs HPGe detectors [69]. The read-out electronics were relatively simple as no coincidence counting or Compton suppression was needed. The details of the read-out electronics as well as the calibration procedure are given in paper 3.

3.4.4 Experimental produced water sample

Furthermore, a salt/water solution was prepared by simply mixing two different salt types, i.e. NaCl and $SrCl_2$, with de-ionized water (H_2O). The resulting element weight fractions as

well as the density of the solution are given in table 3.4. The details of the mixing procedure and the calculation of the mixture density are provided in paper 3.

Table 3.4 The chemical composition and density of the salt/water solution considered in this work.

Elements	Weight fractions	Density of solution (g/cm^3)
Hydrogen	0.107 367	
Oxygen	0.852 122	
Sodium	0.015 641	1.0224
Chlorine	0.024 455	
Strontium	0.000 414	

3.4.5 Measurements

First of all, the natural background was monitored for about 5400 *s* whereas the Cf-252 source was removed from the laboratory. After that, the Cf-252 source was placed in the lead container shown in figure 3.8 and the prompt gamma-rays emerging from the sample were monitored. The experimental prompt gamma-ray spectra as well as the natural background are shown in figure 3.9. It is also important to note that, during the acquisition of the experimental prompt gamma-ray spectrum of the salt/water solution, the lower level discriminator (LLD) of the multi-channel analyzer (MCA) was adjusted in order to avoid monitoring low energy events. More specifically, the LLD value was set to 5.5% which corresponds to ignoring events with energy below 600 keV. This was necessary in order to reduce the dead-time from about 10.0% to about 8.58% which led to a real acquisition time of 46 906.5 s whereas the live acquisition time was 43 200 s. On the other hand, the fact that the spectrum of the natural background was acquired using an LLD value of 2.0% led to the difference in the low energy cut-off for the two spectra (see figure 3.9).

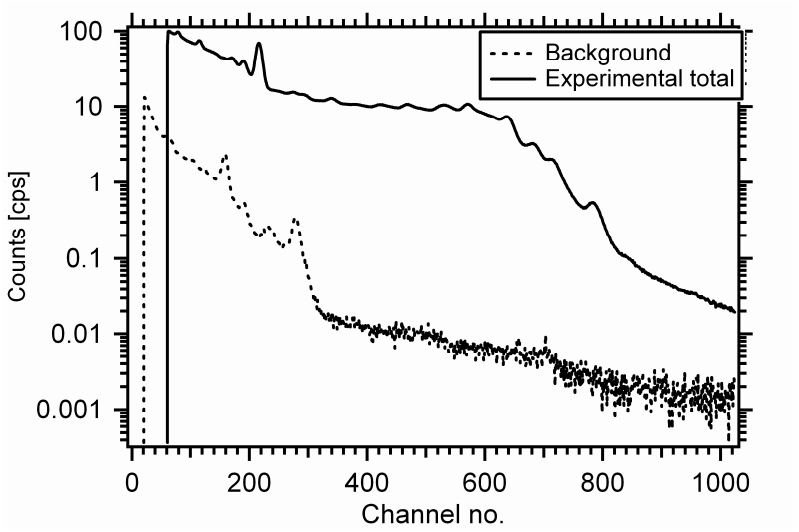

Figure 3.9 The Experimental total prompt gamma-ray spectrum of the salt/water solution whose composition is given in table 3.4. Also shown is the natural background as recorded by the 6 in. x 6 in. NaI detector.

3.4.6 MC simulations

As mentioned earlier in section 3.1, the MCLLS approach was considered for the quantitative analysis. The MCLLS approach is summarized in a stepwise fashion in section 3.3 and papers 3 and 4. In order to perform the LLS search to obtain the amounts of each constituent in the sample, the pertinent prompt gamma-ray libraries of the constituents must be available. The prompt gamma-ray libraries of the constituents were generated through MC simulations using a specific purpose MC code, so-called CEARCPG. CEARCPG is a specific purpose MC code that is capable of generating both singles and coincidence prompt gamma-ray spectra of samples of arbitrary shape and composition. The details of different sampling techniques and variance reduction techniques employed in CEARCPG, as well as benchmark experiments can be found in [42, 43]. The problem geometry shown in figure 3.8 was implemented in CEARCPG and the pertinent elemental prompt gamma-ray libraries were generated assuming a salt/water solution whose composition is given in table 3.5.

Table 3.5 The chemical composition of the salt/water solution used in the MC simulations. Also given is the density of the solution.

Elements	Weight fractions	Density of solution (g/cm^3)
Hydrogen	0.109 606	
Oxygen	0.869 894	
Sodium	0.007 867	1.0112
Chlorine	0.012 356	
Strontium	0.000 277	

The simulated elemental prompt gamma-ray libraries as well as the total background library are given in figure 3.10.

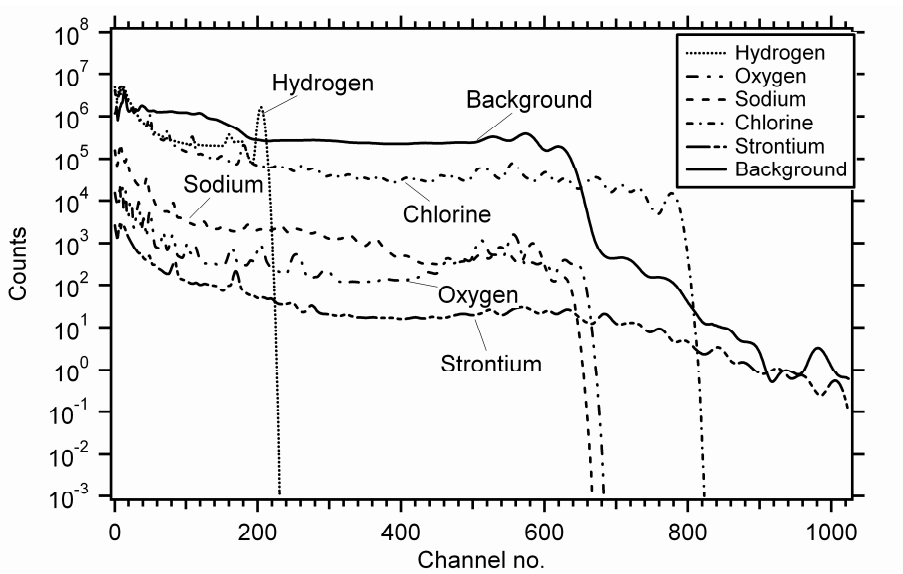

Figure 3.10 Elemental prompt gamma-ray libraries generated using CEARCPG. Also shown is the total background library which is a combination of the contributions from fission gamma-rays that reach the detector, prompt gamma-rays from the surrounding materials, prompt gamma-rays from the activation of the NaI crystal and delayed gamma-rays from Na-24 and I-128.

3.4.7 Quantitative analysis

The next step in the analysis consisted of carrying out the LLS search and the calculation of the amounts of each element in the sample. An important point is, however, the matching of the experimental and simulated spectra prior to carrying out the LLS search. This was, as explained in paper 3, achieved by gain shifting the experimental spectrum and thereby matching the hydrogen peaks in both experimental and simulated spectra [70]. The MCLLS calculated elemental amounts are given in table 3.6.

Table 3.6 MCLLS calculated and real amounts of the elements in the salt/water solution. Also given are the errors in the estimates.

Element	Real weight fraction	Calculated weight fraction	Error [%]
Hydrogen	0.107 367	0.004 2	96.1
Oxygen	0.852 122	-0.98	215.01
Sodium	0.015 641	0.014 3	8.6
Chlorine	0.024 455	0.000 7	97.14
Strontium	0.000 414	0.000 8	92.24

As can be seen in table 3.6, the MCLLS estimates exhibit large errors whereas a negative weight fraction is obtained for oxygen. This is a direct consequence of the fact that the results were obtained using the naïve least-squares approach. However, as mentioned earlier in section 3.3.1, in cases where the covariance matrix to be inverted is ill-conditioned, the results of the naïve least-squares approach will be unreliable. In this case, a high degree of correlation between the background and sodium libraries was observed (a linear correlation coefficient of about 0.824). It was found out that this is directly related to the fact that the background library contains contributions from the activation of the NaI crystal by incident neutrons. On the other hand, it was also pointed out in paper 3 that oxygen has extremely low neutron capture cross-sections at all neutron energies (see figure 3.4). This will lead to a negligible contribution from oxygen to the overall prompt gamma-ray spectrum of the sample. This was also the case for the strontium library due to the small amount of strontium in the sample. It was observed that all these facts led to a significantly high condition number for the covariance matrix (about 9.22×10^5) indicating the fact that the covariance matrix will be strongly ill-conditioned.

The ill-conditioning in the MCLLS approach was treated using the indirect method which is described and discussed in detail in paper 3. It was observed that the implementation of the indirect method, which essentially is based on minimizing the condition number of the covariance matrix by using appropriate combinations of the proper prompt gamma-ray libraries, improves the sensitivity of the MCLLS approach significantly, thus reducing the errors in the MCLLS estimates of the elemental amounts. The results obtained using the indirect method are given in table 3.7

Table 3.7 Real and MCLLS calculated weight fractions of the pertinent elements. In this case, the weight fractions were calculated using the indirect method described in detail in paper 3.

Element	Real weight fraction	Calculated weight fraction	Error [%]
Hydrogen + Oxygen	0. 959 489	0.960 046	0.06
Sodium	0.015 641	0.0152	2.82
Chlorine	0.024 455	0.0241	1.45
Strontium	0.000 414	0.000654	57.8

It is clear from table 3.7 that the MCLLS approach will be a feasible means of quantitative analysis of prompt gamma-ray spectra of produced water samples as long as the assumed and real sample compositions are not too far apart.

4. Discussions and conclusions

Multiphase gas/oil/water/salt monitoring has been and still is a challenging task within the petroleum industry. There is an increasing demand on improved measurement efficiency and accuracy at the same time as the trend is to use subsea installations. As a response to the demands within the offshore oil and gas industry, research on the SOFA concept was initiated by Christian Michelsen Research AS in cooperation with the University of Bergen in 2003 [10-13]. The work presented in this thesis and papers 1-5 focused on one of the key measurement challenges in conjunction with the SOFA concept, i.e. accurate characterization of the produced water component. The most relevant conclusions and discussions on the results of the pertinent work as well as potential future work are presented in this chapter. In order to provide the reader with as good an overview as possible, this chapter is further divided into two sections. In the first section, section 4.1, discussions, conclusions and future work regarding the potential use of GM counters in DMD measurements are presented. Likewise, in section 4.2, the results of the feasibility study investigating the potential use of a PGNAA analyzer in conjunction with the MCLLS approach as an alternative to the DMD measurements are discussed. Also, a discussion on the iterative approach used to treat ill-conditioned cases in the MCLLS approach is given. Furthermore, the conclusions and future work regarding the use of PGNAA for produced water characterization are given in the same section.

4.1 GM counters in DMD measurements

As stated in the introduction of this thesis as well as in chapter 2, the feasibility studies with the DMD measurements for produced water characterization were conducted using CdZnTe semiconductor detectors as these detectors exhibit essentially 100% detection efficiency for 59.5 keV gamma-rays. However, it was also pointed out that a final design based on DMD measurements would benefit from employing gas-filled GM counters. This is mainly due to GM counter's low cost compared with CdZnTe detectors; the fact that GM counters are relatively insensitive to temperature fluctuations and mechanical vibrations and the fact that GM counters require relatively simple read-out electronics. It was also pointed out that stable operation of a radiation gauge in downhole measurements cannot be maintained using CdZnTe detectors due to extremely high temperatures that may be encountered in such harsh environments. In such cases, it would be more advantageous to employ GM counters. The major limitation of GM counters in such applications was identified to be their relatively poor intrinsic gamma-ray detection efficiencies (of the order of 1%). This drastic reduction in the detection efficiency could lead to a smaller SNR. Also, longer integration times would be needed to obtain measurement results with sufficient statistical accuracy. Even more importantly, sources with higher activities would be needed to achieve a certain level of statistical accuracy within a given integration time. In accordance with the ALARA (As Low As Reasonably Achievable) principle, this has the potential to make the use of GM counters in DMD applications for produced water characterization unjustifiable from a radiation safety point of view. For instance, if the counters to be utilized in the DMD measurements had order of magnitude higher gamma-ray detection efficiencies, then the source activity could be reduced by an equal amount to obtain a given statistical accuracy in the measurement results. Therefore, the first part of the work presented in this thesis focused on the identification of a method whereby the poor gamma-ray stopping efficiencies of GM counters could be improved. However, instead of an experimental approach MC simulations were conducted as MC simulations provide a flexibility that may be difficult or impossible to achieve in

laboratory experiments and provide a better insight into the critical parameters affecting the gamma-ray stopping efficiencies of GM counters.

In the study presented in this thesis (see chapter 2) and papers 1, 2 and 5, the focus was on the MC modeling of the intrinsic low energy gamma-ray stopping efficiency of the Centronic ZP1200 GM counter. First of all, MC models of the counter were developed using MCNP5, PENELOPE. These models were used to simulate the intrinsic gamma-ray stopping efficiencies of ZP1200 GM counter at primary photon energy of 59.5 keV. The results obtained using MCNP5 and PENELOPE models of the counter were then compared with experimental stopping efficiency data. It was observed that the MCNP5 and PENELOPE models of the counter showed significant deviation from the experimental data. More precisely, the simulated stopping efficiencies were about half the efficiencies determined experimentally. Possible causes of this severe deviation were discussed and investigated (see paper 1). As a result, the surface porosity of the Cr coating that is plated onto the inner surfaces of the cathode walls was identified as the major cause whereas the approximate treatment of electron transport in general purpose MC codes was identified as rather a minor cause of the severely underestimated stopping efficiencies. The latter was also confirmed through the development of a specific purpose MC code, so-called GMMC, which is one of the major contributions of this work in regards to the MC modeling of the ZP1200 GM counters. GMMC employs, unlike general purpose MC codes, analog or detailed photon/electron transport in the relevant problem geometry. GMMC, MCNP5 and PENELOPE generated stopping efficiency data were compared with experimental stopping efficiency data without taking into account the surface porosity of the inner Cr coating. This comparison was based on a chi-square test of distributions. It was seen that the specific purpose MC code GMMC leads to a slight improvement in the χ_v^2 value (57.4) in comparison with MCNP5 (χ_v^2 = 65.2) and PENELOPE (χ_v^2 = 90.04). Therefore, it was decided to further pursue the use of the specific purpose MC code GMMC.

Especially at low energies, the surface porosity of the Cr coating increases the probability of low energy secondary electrons to penetrate into the fill gas region and cause a Geiger discharge. This was also implemented in the GMMC model of the ZP1200 counter using a density multiplication factor that altered the density of the Cr coating whenever the transport of a secondary electron was to be simulated within this volume. In order to determine an appropriate density multiplication factor, an experimental study was carried out using an uncollimated 10 μCi Am-241 source and an uncollimated detector. This problem geometry was simulated using the GMMC model of the ZP1200 counter for different density multiplication factors. A linear fit to these simulated data yielded a density multiplication factor of about 0.23. In addition, the experiments described in paper 1 and chapter 2 were repeated in order to address the repeatability and positioning issues. GMMC simulations of the ZP1200 counter were repeated using this density multiplication factor to take into account also the surface porosity of the Cr coating. The results of the GMMC simulations were compared with the more recent experimental data as described in chapter 2 and paper 2. It was seen that GMMC simulations that take into account the surface porosity of the Cr coating improved the χ_v^2 value significantly, and a final χ_v^2 value of about 7.0 was obtained. The significant reduction in the χ_v^2 value, therefore, indicates a much better match between the MC simulated and experimental gamma-ray stopping efficiency values.

As explained in chapter 2 (section 2.5) and paper 5, the method considered for enhancement of the gamma-ray stopping efficiencies of ZP1200 GM counters consisted of inserting thin,

insulating disks between the anode wire and the cathode walls of the counter. Incident photons will have substantially low probability of causing a direct ionization the fill gas due to the extremely low density of the fill gas. It was thought that introducing such electrically insulating disks inside the detector would increase the probability of incident photons to undergo collisions while propagating through the fill gas. This would then have the potential to increase the gamma-ray stopping efficiencies of the GM counter through a significant increase in the secondary electron production. GMMC was then utilized in conjunction with the specific purpose MC code PENELOPE and finite element analysis code COMSOL Multiphysics to study the feasibility of introducing thin, non-conducting HfO_2 disks in between the ZP1200 counter's conducting anode wire and cathode walls. The optimal disk thickness was determined to be of the order of 10 μm as this is very close to the maximum range, i.e. the CSDA range, of electrons at the relevant energy range in this material. In these calculations, possibility of introducing several disks inside the counter was also investigated. It was found out that the major limiting factor to the total number of disks would be the optimal distance between each disk. In line with the expectations, the optimal distance is a function of the inelastic mean free path of electrons in the fill gas, and through that, a function of the secondary electron energy. The inelastic mean free path of secondary electrons produced by 59.5 keV photons was calculated to be about 0.21 cm in the fill gas of the ZP1200 counter. Therefore, to minimize the loss of secondary electrons in the solid parts of the counter, the optimal distance between each disk was determined to be of the order of 0.2 cm. In accordance with this observation a total of 15 disks were placed inside the counter and the effective increase in the low energy gamma-ray detection efficiency of the counter was determined to be about threefold. Reducing this distance to half its value, i.e. 0.1 cm, would allow doubling the total number of disks inside the counter. This would lead to production of several more secondary electrons that may penetrate into the fill gas of the counter and lead to a count at the detector output. However, in this case, the effective increase in the efficiency could be lower. That is, the loss of secondary electrons in the solid parts may have the potential of cancelling out the gain and thereby leading to further reduction in the effective increase in the gamma-ray detection efficiency.

Other issues that may need more extensive experimental investigations regarding the use of HfO_2 disks could be summarized as follows:

- potential incompatibility between the disk material and halogen quenched fill gases at elevated temperatures,
- potential distortion of the radial electric field as a result of electrodynamical effects,
- potentially reduced versatility due to mechanical issues.

The MC results reported so far in this thesis and in paper 5 can only be taken as an upper limit to the gain in the low energy gamma-ray stopping efficiencies of ZP1200 counters that can be expected to achieve through insertion of electrically insulating HfO_2 disks. This observation is, however, difficult to justify without extensive experimental data. It is also important to point out that the results of the work presented in this thesis indicate that the maximum achievable gamma-ray detection efficiency in ZP1200 counters is still significantly less than the efficiency of semiconductor and scintillation detectors at the same photon energy.

Consequently, the results of the study presented in this thesis and papers 1, 2 and 5 show that, in the near future, possible utilization of GM counters in the DMD measurement setup of the SOFA concept will remain a challenge. It is also clear from the pertinent results that using the

new concept ZP1200 counter alone may not be sufficient to overcome the challenges associated with poor low energy gamma-ray detection efficiencies. However, it is believed that the possible utilization of GM counters in the DMD measurements should be further investigated, possibly by combining the method proposed in the work presented in this thesis with other methods that may potentially increase the sensitivity of the counter to low energy gamma-rays (see below, section 4.1.1).

4.1.1 Future work on GM counters

In spite of the fact that the simulation results with the new concept ZP1200 GM counter presented so far were obtained using a rigorously benchmarked MC code, in a potential future work, an experimental verification of these results should be carried out. As discussed in the previous section, emphasis should also be given to investigations of the chemical stability of the disk material, i.e., HfO_2, at elevated temperatures, experimental validation of the finite element calculations of the radial static electric field of the GM counter and the mechanical stability of the new concept GM counter.

It is also worth keeping in mind the availability of cylindrical GM counters with platinum (Pt) coatings instead of other low atomic number and density coating materials such as Cr used in ZP1200 counters. These counters are primarily used in harsh environments with high temperatures and mechanical vibrations as Pt exhibits good chemical and mechanical stability. Using higher density and atomic number materials to coat the inner surfaces of cathode walls will increase the sensitivity of the counter to incident gamma-rays. Combining the method of introducing insulating disks inside the counter considered in this work with a counter whose inner cathode surfaces are coated using a material of high atomic number and density could further increase the sensitivity of the counter. As Pt is an expensive metal, to construct a more cost-effective counter, the possibility of using other high atomic number and density metals as the cathode coating could be investigated provided these exhibit a high degree of chemical and mechanical stability. Also, as shown in the work presented in this thesis (see chapter 2), especially at low energies, increasing the inner surface area of the cathode walls will lead to an increase in the number of secondary electrons penetrating into the fill gas and thus, lead to an increase in the overall intrinsic gamma-ray stopping efficiency of the counter. This could also be applied to the insulating disks provided that the distortion of the radial electric field near the disk surfaces would be negligibly small. Increased surface area of the insulating disks may then have the potential to further improve the response of the counter to low energy gamma-rays. Another method of increasing the stopping efficiency is by assembling several small diameter counters in place of a large, single counter [44]. The incident gamma-rays penetrating one of the counters would then have equal probability of being detected in the next counter in the stack. It might be worthwhile to study the low energy gamma-ray response of such assembly of small diameter GM counters in which all of the counters in the assembly are in addition modified by inclusion of a sufficient number HfO_2 disks.

It would also be of scientific interest to investigate the intrinsic gamma-ray stopping efficiencies of ZP1200 GM counters at other primary gamma-ray energies as, to the best of the author's knowledge, such information is yet to be reported. The response of the counter at other gamma-ray energies could be first simulated and then benchmarked with experimental data.

4.2 PGNAA in conjunction with the MCLLS approach as an alternative to DMD measurements

As discussed in the introduction to this thesis as well as throughout chapter 3, the DMD measurements show extreme sensitivity to salinity of produced water samples. Therefore, it could be concluded that the DMD measurement principle is possibly an adequate approach in applications where only information on salinity is required. However, in applications where more information on produced water samples such as accurate chemical/elemental compositional analysis is required, the DMD measurements alone cannot be used. This is because the measurements of transmitted and scattered gamma-rays in produced water samples, are not sufficiently sensitive for providing detailed information on the chemical/elemental composition of arbitrary salt/water mixtures unless these are used in combination with other measurement modalities such as permittivity and ultrasound measurements.

On the other hand, the PGNAA method is a well-known elemental/isotopic analysis technique that is based on bombarding a sample of interest with neutrons and monitoring the energies of the resultant prompt gamma-rays which are characteristic of every element and every isotope of every element using an energy sensitive radiation detector such as a semiconductor or a scintillator. PGNAA has found many industrial applications such as characterization of vitrified waste, analysis of coal and cement samples [21-24]. Furthermore, elemental analysis by the use of PGNAA represents an inverse problem in the sense that the outcome of the pertinent measurement, i.e., the pulse height distribution of the prompt gamma-rays, is available whereas the critical parameters that determine the shape of the resulting pulse height distribution, i.e., the chemical composition of the sample, need to be estimated. For this purpose, the so-called single peak analysis is often employed as the quantitative analysis tool in many radiation analyzers based on PGNAA. As a summary, the single peak analysis is based on examining the resulting gamma-ray spectra to identify the relevant photopeaks; based on the energies of these photopeaks determining the elements that are present in the sample under investigation; and calculating the amounts of each element in the sample based on the integral number of counts in these photopeaks. In a work by Gardner et. al. [72], however, it was shown that the use of LLS analysis would increase the sensitivity of the subsequent quantitative analysis by a factor of 2.5 in comparison with the single peak analysis method. This is mainly due to the fact that the LLS analysis utilizes the whole spectrum information instead of utilizing only the photopeaks in the spectrum. On the other hand, the major drawback of the LLS analysis would be the fact that the elemental libraries must be known prior to carrying out the pertinent calculations. The elemental libraries could be determined experimentally. Nevertheless, this would make the LLS analysis significantly impractical. To overcome this limitation, the use of MCLLS approach was proposed in which the pertinent elemental/component libraries are generated using accurate forward MC simulations. PGNAA in conjunction with the MCLLS approach was applied to different measurement systems confirming the accuracy of this approach [5, 9, 27]. At this point, it should be mentioned that the MCLLS approach can be utilized in conjunction with not only prompt gamma-ray spectra, but also with other spectral analysis methods such as energy dispersive X-ray fluorescence (EDXRF). Examples of this can be found in [76]. Recently, it was shown by Wang et. al. [5] that PGNAA in conjunction with the MCLLS approach could be successfully applied to the hydrocarbon multiphase flow measurement problem in which the parameters of interest are the weight fractions of the gas, oil, water and salt phases. This recent development prompted an interest in considering PGNAA in conjunction with the

MCLLS approach as an alternative to the currently pursued DMD measurements in the SOFA concept.

The MCLLS technique has several advantages over the more traditional single peak analysis technique. These are listed in chapter 3 of this thesis. As far as its limitations are concerned, on the other hand, the most obvious one is in that the technique requires time consuming MC simulations to be carried out in order to generate the pertinent elemental/compound libraries. MC simulations could, however, be accelerated by extensive use of variance reduction techniques as well as by making use of parallel computing techniques. Another important limitation of the technique which may, in some cases, lead to severe sensitivity deterioration was identified to be the ill-conditioning in the covariance matrix which has to be inverted in the LLS search. It has come to the author's attention that this severe limitation lacked a rigorous treatment. As described in paper 4 and chapter 3, another important contribution of the work presented in this thesis is the proper treatment of the ill-conditioned cases in the MCLLS approach. Ill-conditioning in the MCLLS approach will depend on several different factors such as the choice of radiation detectors, high degree of linear correlation between any of the libraries and negligible contribution from one library to the overall prompt gamma-ray spectrum. This will lead to a highly uncertain solution to the set of linear equations and thus, may impair the sensitivity of the MCLLS approach in such cases. In certain cases, the ill-conditioning in the MCLLS approach could be reduced by proper choice of detectors, i.e. by using detectors with better energy resolution to avoid overlapping peaks in the spectrum. However, in this work, a more robust and cost-effective solution to the problem of ill-conditioned cases in the MCLLS approach is identified. The proposed solution is an iterative approach that is based on minimizing the condition number of the covariance matrix in the LLS search. This could also be interpreted as a modification of the original MCLLS approach and can, in a stepwise fashion, be given as follows:

1) For each constituent, construct two libraries where one library is a single constituent and the other is the sum of the rest of the constituents.
2) For each case, examine the condition number of the covariance matrix.
3) Choose the fit that yields the lowest condition number.
4) Repeat steps 1) - 3) against the residual obtained from the best fit that yielded the lowest condition number and remove the library of the single constituent.

The proposed iterative approach was applied to the MC simulated multiphase flow measurement problem previously treated by Wang et. al.[5]. In the MC simulations, it was assumed that the samples were bombarded using a Cf-252 neutron source whereas the resulting prompt gamma-rays were monitored using a large, 6 in. x 6 in. NaI scintillation detector. The multiphase flow measurement problem was chosen as an example as it was identified as a particularly difficult problem where all libraries with the exception of salt and background will be linearly correlated since oil, gas and water libraries are dominated by the contribution from hydrogen. In addition, the oil and gas libraries will have the same spectral shape as both contain varying amounts of carbon and hydrogen. This means that the ill-conditioning could not be avoided even if high energy resolution HPGe semiconductor detectors are used instead of the NaI scintillation detectors. It should, however, be stressed and made clear to the reader that the intention of the study was not addressing the issues related to the challenges in connection with multiphase flow measurements. The intention was rather to demonstrate the feasibility of the proposed iterative solution for treating ill-conditioned cases in the MCLLS approach.

As presented in paper 4, the condition number of the covariance matrix, in the case where all libraries (oil, gas, water, salt and background) were fitted individually in the LLS analysis, was determined to be 2.61×10^{6}. The large condition number is a clear indication of the fact that the least-squares solution will be unstable and will produce large uncertainties. Large uncertainties caused by ill-conditioning in the MCLLS approach were also encountered in the work by Wang et. al.[5]. Thereafter, the iterative approach proposed in this work was applied to the highly ill-conditioned multiphase flow measurement problem and it was seen that this approach proves to be a feasible means of treating the ill-conditioning in this particular problem. Also, it is expected that the iterative approach could be utilized in other ill-conditioned cases.

As mentioned earlier, another major objective in the work presented in this thesis is the demonstration of the feasibility of applying PGNAA in conjunction with the MCLLS approach for subsea produced water characterization. For this purpose, an experimental study was conducted. A salt/water solution was prepared by mixing two different salts, NaCl and $SrCl_2$, with de-ionized water. The solution was poured into an Al container and was exposed to a 1μg Cf-252 spontaneous fission neutron source. The resulting prompt gamma-ray spectrum was recorded using a 6 in. x 6 in. NaI scintillation detector. The measurement live-time was about 43200 s. The lower level discriminator (LLD) of the multi-channel analyzer (MCA) was configured so as to reduce the dead-time to about 8.58% . A specific purpose MC code, CEARCPG, was used to generate the elemental library spectra. Using CEARCPG the elemental library spectra were generated for a salt/water solution with slightly different chemical composition (see section 3.4 and paper 3). It is a well-known fact that PGNAA suffers from low SNR values and it soon became evident that, for the subsequent quantitative analysis to be as accurate as possible, a carefully determined background library also had to be taken into account. In accordance with the MCLLS approach, the elemental library spectra as well as the background library were then fitted against the experimental prompt gamma-ray spectrum of the salt/water solution representing the "unknown" produced water sample. However, it was observed that the results of the naïve LLS search was rather poor in the sense that the calculated amounts of all elements in the sample showed significant deviation from the real amounts. Further investigations revealed that this is related to the ill-conditioning of the covariance matrix (whose condition number was calculated to be about 9.22×10^{5}). The causes of the ill-conditioning were identified to be the linear correlation between the sodium and background libraries; the extremely low neutron capture cross-section of oxygen at all neutron energies; and the negligible contribution from strontium to the overall prompt gamma-ray spectrum as a result of its low neutron capture cross-section and the fact that only a small amount of strontium is present in the sample. The ill-conditioning in the MCLLS approach was treated through the use of the indirect approach briefly introduced in chapter 3 (section 3.3.1) and described in detail in paper 3. It was seen that the application of the indirect approach improved the results of the MCLLS approach significantly by searching for combinations of the existing libraries that minimize the condition number of the covariance matrix in the LLS search. As shown in chapter 3 (section 3.4) and paper 3, amounts of hydrogen, oxygen, sodium and chlorine in the sample were determined with good accuracy whereas the error in the calculated amount of strontium was of the order of 57.8% with respect to its real amount in the sample. This could be explained by both the substantially low amount of strontium in the sample as well as pulse pile-up effects at higher energies in the experimental spectrum which are not present in the MC simulated spectra. This was further investigated by eliminating a range of channels in the LLS search. In this case, channels 800-1024 were excluded in the calculations. It was observed that excluding channels 800-1024 in the LLS search further improved the calculated amount of strontium as the error was reduced

to about 15.94%. The change in the calculated amount of strontium indicates that the pulse pile-up in experimental prompt gamma-ray spectra may become an important source of error. This could, however, be eliminated by either correcting the experimental spectrum for pulse pile-up, or including effects of pulse pile-up in the simulated library spectra [77]. It is also important to point out the fact that the indirect approach used in this study to treat the ill-conditioning in the MCLLS approach is no longer pursued due to its recursive nature that could lead to higher uncertainties in the calculated amounts of the pertinent components. As a reminder, a more rigorous discussion on this is given in paper 4 and chapter 3. Consequently, the results of the experimental work presented in this thesis and in paper 3 indicate that the PGNAA method in conjunction with the MCLLS approach would be feasible for the characterization of produced water samples.

As can be seen, the MCLLS approach constitutes an important part of a potential analyzer based on PGNAA for characterization of produced water samples. Any limitations of the MCLLS approach would have direct consequences for the final design of such analyzers as it is used for the subsequent quantitative analysis. Inaccuracies or weaknesses of the MCLLS approach would impair the sensitivity in the quantitative analysis or, in the worst case, make the quantitative results entirely meaningless. As stated above, this is going to be the case whenever the covariance matrix is ill-conditioned. However, the iterative approach proposed in the work presented in this thesis could be utilized to improve the sensitivity of the MCLLS approach in such ill-conditioned cases. This was also demonstrated through the example of highly ill-conditioned multiphase flow measurement problem. Adequate treatment of the ill-conditioned cases in the MCLLS approach also has some important practical implications. The usual practice in such cases has been to leave out a few problematic libraries and execute the LLS search with the remaining libraries. Nonetheless, this does not allow a full analysis of the sample of interest. In order to perform full analysis, it is, in some cases, suggested to combine PGNAA with other measurement techniques. This approach reduces the cost-effectiveness of a PGNAA analyzer, and leads to a more complex gauge design. In some instances, use of PGNAA analyzers in combination with other nucleonic gauges is considered. The major disadvantage of this approach would be the increase in the background in the experimental prompt gamma-ray spectra as well as an increase in the radiation dose to the environment which is in disagreement with the ALARA principle. The proposed iterative approach, on the other hand, offers a more cost-effective and safer alternative to these solutions considered earlier. Even more importantly, the applications of MCLLS approach are not limited to PGNAA method; it can also be used as an appropriate quantitative analysis technique in other spectral analysis methods. It can, therefore, be concluded that the results presented in this thesis and in paper 4 indicate that the iterative approach may be sufficiently adequate to treat ill-conditioned cases in the MCLLS approach for inverse radiation analyzers, and that its utilization should be pursued in future applications of the MCLLS approach.

4.2.1 Future work on PGNAA in conjunction with the MCLLS approach

In the near future, the proposed iterative approach should be subject to several more tests although it was successful in improving the sensitivity of the MCLLS approach in the extreme case of multiphase flow measurement where almost all pertinent component libraries are linearly correlated. This should be done in order to investigate its performance under different conditions and with noisier experimental data. This is mainly because any unforeseen sources of noise (background) contributing to the experimental spectrum would affect the performance of both the MCLLS approach and the iterative approach in a negative sense. It is a well-known fact that more sophisticated detection techniques such as coincidence counting

and Compton suppression (or anti-coincidence) techniques are used to suppress the overall background in applications of the PGNAA method. It could also be investigated as to whether or not the iterative approach could further improve the sensitivity of the MCLLS approach in cases where its use is considered in conjunction with these detection techniques.

The experimental study conducted and presented in this thesis showed that PGNAA in conjunction with the MCLLS approach would be feasible for characterization of produced water samples provided the ill-conditioning in the MCLLS approach can be treated properly. The overall background in the final PGNAA spectrum will partly depend on the surrounding structures as neutrons scattered from the sample as well as primary neutrons from the source that are not incident on the sample may activate the nuclei in these structures and, in turn, produce unwanted prompt gamma-rays that reach the detector. The intensity of these gamma-rays can be reduced by proper shielding of the detector. However, their contribution cannot be totally eliminated. Therefore, in a future work, it would be of practical interest to test the system in seawater or similar surroundings as the analyzer is being designed for use in subsea installations. This is important as the content of H_2O and salt ions dissolved in water may change the overall background in the measurements. In this case, the ill-conditioning in the MCLLS approach could be even more severe as both the background and signal may contain contributions from the same elements. Since the background and signal may, in such cases, be linearly correlated, the use of the iterative approach proposed in this work may have critical importance for proper gauge performance.

References

[1] JOHANSEN, G. A. & JACKSON, P. 2004. *Radioisotope Gauges for Industrial Process Measurements,* Chichester, West Sussex, England, John Wiley & Sons, Ltd.

[2] HOLSTAD, M. B. 2000. *Implementation of Dual Mode Gamma-ray Densitometer for Gas Fraction Measurement in Multiphase Pipe Flows.* M.Sc. thesis, University of Bergen, Norway.

[3] TJUGUM, S. A., FRIELING, J. & JOHANSEN, G. A. 2002. A compact low energy multibeam gamma-ray densitometer for pipe-flow measurements. *Nucl. Instr. and Meth. B,* **197,** 301-309.

[4] PARK, H. S. & CHUNG, C. H. 2007. Design and Application of a Single-Beam Gamma Densitometer for Void Fraction Measurement in a Small Diameter Stainless Steel Pipe in a Critical Flow Condition. *Nucl. Eng. Technol.,* **39,** 349-358.

[5] WANG, J., LI, F. & GARDNER, R. P. 2008. On the Use of Prompt Gamma-ray Neutron Activation Analysis for Determining Phase Amounts in Multiphase Flow. *Meas. Sci. Technol.,* **19,** 094005.

[6] TJUGUM, S. A., JOHANSEN, G. A. & HOLSTAD, M. B. 2001. The Use of Gamma Radiation in Fluid Flow Measurements. *Radiat. Phys. Chem.,* **61,** 797-798.

[7] JOHANSEN, G. A. & JACKSON, P. 2000. Salinity Independent Measurement of Gas Volume Fraction in Oil/Gas/Water Pipe Flows. *Appl. Radiat. Isotopes,* **53,** 595-601.

[8] GARDNER, R. P. & SOOD, A. 2010. On the Future of Monte Carlo Simulation for Nuclear Logs. *Appl. Radiat. Isotopes,* **68,** 932-935.

[9] GARDNER, R. P., HAN, X. & GUO, P. On Using Monte Carlo Generated Libraries for Applying the Library Least-Squares Analysis Approach to the C/O Tool. *SPWLA 47th Annual Logging Symposium*, June 4-7 2006 Veracruz, Mexico. SPWLA.

[10] BRUVIK, E. M., HOLSTAD, M. B., SPILDE, J., HJERTAKER, B. T., STAVLAND, S. H., FRØYSA, K. E. & MEYER, S. K. Fluid Characterisation in a Subsea On-line Multiphase Fluid Sampling and Analysis System. *27th International North Sea Flow Measurement Workshop*, October 20-23 2009 Tønsberg, Norway.

[11] BAKER, A., BJELLAND, C., SPILDE, J., FRØYSA, K. E., HOLSTAD, M. B., JOHANSEN, G. A., HJERTAKER, B. T., BERNTSEN, B. & STAVLAND, S. H. A Novel Subsea On-line Multiphase Fluid Sampling and Analysis System. *5th World Congress on Industrial Process Tomography*, September 3-6 2007 Bergen, Norway.

[12] BRUVIK, E. M., HJERTAKER, B. T. & HALLANGER, A. 2010. Gamma-ray tomography applied to hydro-carbon multi-phase sampling and slip measurements. *Flow Meas. Instrum.,* **21,** 240-248.

[13] HOLSTAD, M. B. & JOHANSEN, G. A. 2005. Produced water characterization by dual modality gamma-ray measurements. *Meas. Sci. Technol.,* **16,** 1007-1013, doi:10.1088/0957-0233/16/4/013.

[14] VEIL, J. A., PUDER, M. G., ELCOCK, D. & REDWEIK, R. J. J. 2004. A white paper describing produced water from production of crude oil, natural gas and coal bed methane. Available: http://fossil.energy.gov/programs/oilgas/publications/.

[15] THORN, R., JOHANSEN, G. A. & HAMMER, E. A. 1997. Recent developments in three-phase flow measurement. *Meas. Sci. Technol.,* **8,** 691-701.

[16] JOHANSEN, G. A. & TJUGUM, S. A. Fluid composition analysis by multiple gamma-ray beam and modality measurements. *25th International North Sea Flow Measurement Workshop*, October 16-19 2007 Oslo, Norway.

[17] BERNTSEN, B. 2005. *Utvikling av målekammer for karakterisering av saltvann ved bruk av absorpsjon og spredning av gammastråling.* M.Sc. Thesis, University of Bergen, Norway (in Norwegian).

[18] JOHANSEN, G. A., VAGLE, O., OLSEN, Ø., HOLSTAD, M. B. & MERIC, I. Geiger-Müller detectors for gamma-ray tomography. *5th International Symposium on Process Tomography*, August 25-26 2008 Zakopane, Poland.

[19] KNOLL, G. 2000. *Radiation Detection and Measurement,* USA, John Wiley & Sons, Ltd.

[20] CENTRONIC Databook on Geiger Müller Tubes. Croydon, UK: Centronic.

[21] MOLNÀR, G. L. 2004. *Handbook of Prompt Gamma Activation Analysis with Neutron Beams,* Dordrecht, The Netherlands, Kluwer Academic Publishers.

[22] LIM, C. S. 2004. Recent developments in neutron-induced gamma activation for on-line multielemental analysis in industry. *J. Radioanal. Nucl. Ch.,* **262,** 525-532.

[23] BORSARU, M. & JECNY, Z. 2001. Application of PGNAA for bulk coal samples in a 4π geometry. *Appl. Radiat. Isotopes,* **54,** 519-526.

[24] LIM, C. S. & ABERNETHY, D. A. 2005. On-line coal analysis using fast neutron-induced gamma-rays. *Appl. Radiat. Isotopes,* **63,** 697-704.

[25] ARINC, F., GARDNER, R. P., WIELOPOLSKI, L. & STILES, A. R. 1975. Application of the least-squares method to the analysis of XRF spectral intensities from atmospheric particulates collected on filters. *Adv. X Ray Anal.,* **19,** 367-379.

[26] VERGHESE, K., GARDNER, R. P., MICKAEL, M., SHYU, C. M. & HE, T. 1988. The Monte Carlo-library Least Squares Analysis Principle for Borehole Nuclear Well Logging Elemental Analyzers. *Nucl. Geophys.,* **2,** 183-190.

[27] SHYU, C. M., GARDNER, R. P. & VERGHESE, K. 1993. Development of the Monte Carlo-Library Least-Squares Method of Analysis for Neutron Capture Prompt Gamma-ray Analyzers. *Nucl. Geophys.,* **7,** 241-267.

[28] DUPREE, S. A. & FRALEY, S. K. 2002. *A Monte Carlo Primer: A Practical Approach to Radiation Transport* New York, NY, Kluwer Academic/Plenum Publishers.

[29] LUX, I. & KOBLINGER, L. 1991. *Monte Carlo Transport Methods, Neutron and Photon Calculations,* Boca Raton, FL, USA, CRC Press Inc.

[30] CARTER, L. L. & CASHWELL, E. D. 1975. *Particle - Transport Simulation with the Monte Carlo Method,* Oak Ridge, TN, USA, USERDA Technical Information Center.

[31] THE, FLUKA COLLABORATION 2011. FLUKA: A Multi-Particle Transport Code. Geneva.

[32] NELSON, W. R., HIRAYAMA, H. & ROGERS, D. W. O. 1985. The EGS4 Code System.

[33] GEANT4 COLLABORATION 2003. GEANT4 - a simulation toolkit. *Nucl. Instr. and Meth. A,* 506**,** 250-303.

[34] CULLEN, D. E. 2005. TART2005 - A Coupled Neutron-Photon 3-D, Combinatorial Geometry, Time Dependent Monte Carlo Transport Code.

[35] X5 MONTE, CARLO TEAM 2003. A General Monte Carlo N-Particle Transport Code, Version 5. Los Alamos, NM, USA: Los Alamos National Laboratory.

[36] SALVAT, F., FERNANDEZ-VAREA, J. M. & SEMPAU, J. 2006. PENELOPE 2006: A Code System for Monte Carlo Simulation of Electron and Photon Transport. France: OECD.

[37] EATKINS, J. 2009. On the Effect of Updated MCNP Photon Cross Section Data on the Simulated Response of the HPA TLD. *Radiat. Prot. Dosim.,* **134,** 66-71.

[38] ZAMBURLINI, M., BYUN, S. H., PEJOVIC-MILIC, A., PRESTWICH, W. V. & CHETTLE, D. R. 2007. Evaluation of MCNP5 and EGS4 for the simulation of in vivo strontium XRF measurements. *X-ray Spectrom.,* **36,** 76-81.

[39] SEMPAU, J., ACOSTA, E., BARO, J., FERNÀNDEZ-VAREA, J. M. & SALVAT, F. 1997. An algorithm for Monte Carlo simulation of coupled electron-photon transport. *Nucl. Instr. and Meth. B,* **132,** 377-390.

[40] CARVAJAL, M. A., GARCÍA-PAREJA, S., GUIRADO, D., VILCHES, M., ANGUIANO, M., PALMA, A. J. & LALLENA, A. M. 2009. Monte Carlo simulation using the PENELOPE code with an ant colony algorithm to study MOSFET detectors. *Phys. Med. Biol.,* **54,** 6263-6276.

[41] VILCHES, M., GARCÍA-PAREJA, S., GUERRERO, R., ANGUIANO, M. & LALLENA, A. M. 2008. Monte Carlo simulation of the electron transport through air slabs: A comparative study of PENELOPE, GEANT3, Geant4 and EGSnrc Monte Carlo codes. *IEEE Trans. Nucl. Sci.,* **55,** 710-716.

[42] HAN, X. 2005. *Development of Monte Carlo code for Coincidence Prompt Gamma-ray Neutron Activation Analysis.* PhD Thesis, North Carolina State University, USA.

[43] HAN, X. & GARDNER, R. P. 2007. The Monte Carlo code CEARCPG for coincidence prompt gamma-ray neutron activation analysis. *Nucl. Instr. and Meth. B,* **263,** 320-325.

[44] FRIEDMAN, H. Geiger Counter Tubes. *Proceedings of the I.R.E. - Waves and Electrons Section*, 1949.

[45] VAGLE, O., OLSEN, Ø. & JOHANSEN, G. A. 2007. A simple and efficient active quenching circuit for Geiger-Müller counters. *Nucl. Instr. and Meth. A,* **580,** 358-361.

[46] WATANABE, T. 1999. A computational analysis of intrinsic detection efficiencies of Geiger-Mueller tubes for photons. *Nucl. Instr. and Meth. A,* **438,** 439-446.

[47] DUNN, W. L. & GARDNER, R. P. 1972. The determination of intrinsic gamma-ray detection efficiencies for cylindrical Geiger-Müller tubes by Monte Carlo methods. *Nucl. Instr. and Meth.,* **103,** 373-384.

[48] HJERTAKER, B. T., JOHANSEN, G. A. & JACKSON, P. 2001. Level measurement and control strategies for subsea separators. *J. Electron. Imaging,* **10,** 679-689.

[49] LEES, R. P. 2002. Increasing control and accuracy in the separation process by density profiling. *Meas. Control,* **35,** 164.

[50] LAZURIK, V., MOSKVIN, V. & TABATA, T. 1998. Average depths of electron penetration: Use as characteristic depths of exposure. *IEEE Trans. Nucl. Sci.,* **45,** 626-631.

[51] SOOD, A. & GARDNER, R. P. 2004. A new Monte Carlo assisted approach to detector response functions. *Nucl. Instr. and Meth. B,* **213,** 100-104.

[52] BEVINGTON, P. R. & ROBINSON, D. K. 2003. *Data Reduction and Error Analysis for the Physical Sciences,* New York, NY, USA, McGraw-Hill.

[53] SVATOS, M. M. 1998. *The Macro Response Monte Carlo Method for Electron Transport.* PhD Thesis, University of California, USA.

[54] BALLINGER, C. T., CULLEN, D. E., PERKINS, S. T., RATHKOPF, J. A., MARTIN, W. R. & WILDERMAN, S. J. 1992. Single-scatter Monte Carlo compared to condensed history results for low energy electrons. *Nucl. Instr. and Meth. B,* **72,** 19-27.

[55] X-5 MONTE CARLO TEAM Criticality Calculations with MCNP5: A Primer. GOORLEY, T. (ed.). Los Alamos, NM, USA: Los Alamos National Laboratory.

[56] L'ECUYER, P. 1988. Efficient and portable combined random number generators. *Commun. ACM,* **31,** 742-749.

[57] CULLEN, D. E., HUBBELL, J. H. & KISSEL, L. 1997. EPDL97: The Evaluated Photon Data Library '97 Version. Livermore, USA: Lawrence Livermore National Laboratory.

[58] PERSLIDEN, J. 1983. A Monte Carlo program for photon transport using analogue sampling of scattering angle in coherent and incoherent scattering processes. *Comput. Prog. Biomed.,* **17,** 115-128.

[59] CARRON, N. J. 2007. *An Introduction to the Passage of Energetic Particles Through Matter,* Boca Raton, FL, USA, CRC Press Taylor & Francis Group.

[60] PERKINS, S. T., CULLEN, D. E. & SELTZER, S. M. 1991. Tables and Graphs of Electron-Interaction Cross Sections from 10 eV to 100 GeV Derived from the LLNL Evaluated Electron Data Library (EEDL), Z=1-100. Livermore, CA, USA: Lawrence Livermore National Laboratory.

[61] CALDERON, A. F. 2012. Personal communication, North Carolina State University, USA.

[62] BERGER, M. J., HUBBELL, J. H., SELTZER, S. M., CHANG, J., COURSEY, J. S., SUKUMAR, R., ZUCKER, D. S. & OLSEN, K. 2010. XCOM: Photon Cross Section Database, Version 1.5. Gaithersburg, MD, USA: National Institute of Standards and Technology.

[63] BERGER, M. J., COURSEY, J. S., ZUCKER, M. A. & CHANG, J. 2005. Stopping-Power and Range Tables for Electrons, Protons, and Helium Ions, Version 1.2.3. Gaithersburg, MD, USA: National Institute of Standards and Technology.

[64] COMSOL AB 2010. Introduction to COMSOL Multiphysics, Version 4.0 a. USA: COMSOL AB.

[65] SEABURY, E. H. & CAFFREY, A. J. 2006. Explosives Detection and Identification by PGNAA. Idaho Falls, Idaho, USA: Idaho National Laboratory.

[66] IM, H. J. & SONG, K. 2009. Applications of Prompt Gamma Ray Neutron Activation Analysis: Detection of Illicit Materials. *Appl. Spectrosc. Rev.,* **44,** 317-334.

[67] RINARD, P. 1991. Neutron Interactions with Matter. REILLY, D., ENSSLIN, N. & JR., H. S. (eds.) *Passive Nondestructive Assay of Nuclear Materials.* Nuclear Regulatory Comission.

[68] NNDC EVALUATED NUCLEAR DATA FILE (ENDF) Retrieval and Plotting. Brookhaven National Laboratory.

[69] PROCTOR, R., YUSUF, S., MILLER, J. & SCOTT, C. 1999. Detectors for on-line prompt gamma neutron activation analysis. *Nucl. Instr. and Meth. A,* **422,** 933-937.

[70] GARDNER, R. P., SAYYED, E., ZHENG, Y., HAYDEN, S. & MAYO, C. W. 2000. NaI detector neutron activation spectra for PGNAA applications. *Appl. Radiat. Isotopes,* **53,** 483-497.

[71] SALMON, L. 1962. Analysis of gamma-ray scintillation spectra by the method of least squares. *Nucl. Instr. and Meth.,* **14,** 193-199.

[72] GARDNER, R. P., SOOD, A., WANG, Y. Y., LIU, L., GUO, P. & GEHRKE, R. J. 1997. Single peak versus library least-squares analysis methods for the PGNAA analysis of vitrified waste. *Appl. Radiat. Isotopes,* **48,** 1331-1335.

[73] WONG, S. S. M. 1997. *Computational Methods in Physics and Engineering,* Singapore, World Scientific Publishing CO. PTE, LTD.

[74] ASTER, R. C., BORCHERS, B. & THURBER, C. H. 2005. *Parameter Estimation and Inverse Problems,* Burlington, MA, USA, Elsevier Academic Press.

[75] CLINE, A. K., MOLER, C. B., STEWART, G. W. & WILKINSON, J. H. 1979. An estimate for the condition number of a matrix. *SIAM J. Numer. Anal.,* **16,** 368-375.

[76] GARDNER, R. P. & XU, L. 2009. Status of the Monte Carlo library least-squares (MCLLS) approach for non-linear radiation analyzer problems. *Radiat. Phys. Chem.,* **78,** 843-851.

[77] GUO, W., LEE, S. H. & GARDNER, R. P. 2004. The Monte Carlo approach MCPUT for correcting pile-up distorted pulse-height spectra. *Nucl. Instr. and Meth. A,* **531,** 520-529.

APPENDIX 1: List of GMMC subroutines and modules

Modules:

bank_module.f90 → Module used for banking the secondary particles.

geometry_module.f90 → Module used for storing geometric parameters.

global_module.f90 → Module used for storing global constants and variables.

random_module.f90 → Module used for random number generation.

transport_module.f90 → Module containing particle transport parameters.

xs_module.f90 → Module containing photon/electron cross-section data.

Subroutines:

bremsstrahlung.f90 → Subroutine used for sampling of electron average energy loss in Bremsstrahlung events.

caldist.f90 → Subroutine used to calculate the distance from the source particle position to the detector surface.

calemfp.f90 → Subroutine used to sample the electron path length to the next interaction site.

calexs.f90 → Subroutine used to calculate the electron macroscopic cross-sections.

calgeo.f90 → Subroutine used to calculate pertinent geometry variables.

calpmfp.f90 → Subroutine has the same function as calemfp.f90. However, in this case, the distance is sampled for photons.

calpxs.f90 → Subroutine has the same function as calexs.f90. However, in this case, the photon macroscopic cross-sections.

chemistry.f90 → Subroutine used to calculate the atomic weight fractions of elements in a given material.

compton.f90 → Subroutine used to sample the energy loss and scattering angle of photons in Compton (incoherent) scattering events.

direct.f90 → Subroutine used to determine the change of direction of particles.

elastic_scattering.f90 → Subroutine used to sample the scattering angle of electrons in elastic scattering events.

element.f90 → Subroutine used to sample the colliding element in a material consisting of several elements.

excitation.f90 → Subroutine used to sample the electron average energy loss in excitation events.

geotest.f90 → Subroutine used to calculate the distance to the nearest interface from the particle's current position. This subroutine also checks whether or not the distance to the nearest interface is greater than the sampled distance to the next interaction site.

gmmc.f90 → Main steering program.

input.f90 → Subroutine used to read the input file.

interaction.f90 → Subroutine used to sample the interaction type.

ionization.f90 → Subroutine used to sample the electron energy loss ionization events. This subroutine also calculates the scattering angle based on two-body kinematics.

photoelectric.f90 → Subroutine used to model photoelectric absorption events. This is also where the secondary photoelectrons are stored in the secondary stack.

pmove.f90 → Subroutine used to move the particle to either the next interaction site or the nearest interface by updating its position coordinates.

print_input.f90 → Subroutine used to print pertinent input parameters in a separate text file.

range_rejection.f90 → Subroutine used to implement the range rejection technique for secondary electron transport.

rayleigh.f90 → Subroutine used to sample the scattering angle of photons in Rayleigh (coherent) scattering events.

read_xs.f90 → Subroutine used to read pertinent photon/electron cross-section data from the ENDF files.

secstack.f90 → Subroutine used to extract phasespace parameters of secondary electrons from the secondary stack.

slocate.f90 → Subroutine used to locate source particle position. This subroutine is also used to implement the source biasing technique.

source.f90 → Subroutine used to set initial source particle parameters.

store.f90 → Subroutine used to store phasespace parameters of secondary electrons in the secondary stack.

APPENDIX 2: Fortran 90 implementation of the L'Ecuyer random number generator

```
module random_number_generator

  implicit none
  integer :: iseed1,iseed2  ! Random number generator seeds

  contains

  function rand(dummy)

    integer :: dummy,i1,i2,iz
    real, parameter :: uscale=1.0/2.147483563e+9
    real :: rand

    i1=iseed1/53668
    iseed1=40014*(iseed1-i1*53668)-i1*12211
    if(iseed1<0) iseed1=iseed1+2147483563

    i2=iseed2/52774
    iseed2=40692*(iseed2-i2*52774)-i2*3791
    if(iseed2<0) iseed2=iseed2+2147483399

    iz=iseed1-iseed2
    if(iz<1) iz=iz+2147483562
    rand=iz*uscale

    return
  end function rand

end module random_number_generator
```

APPENDIX 3: Example of boundary calculations in GMMC

For this example let us assume a particle propagating in an infinite, uniform medium with given density and material composition, i.e. medium 1 in figure A3.1. Also, assume that non-uniformity is introduced in this geometry in the form of a spherical region, with 1 cm radius, which is located at the origin of the Cartesian coordinate system. It is assumed that this region contains a different material with different density and material composition, i.e. medium 2 in figure A3.1. This example and the following calculations are very similar to the example given in [ref.].

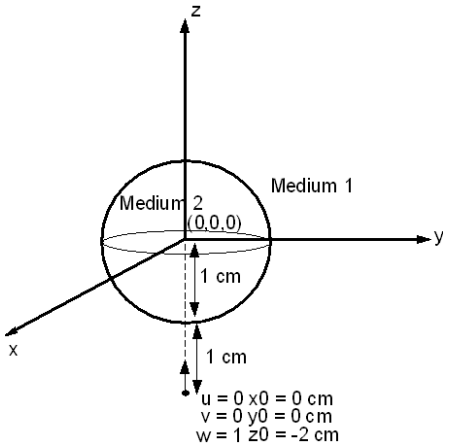

Figure A3.1 **Sketch of a particle propagating in an infinite and uniform medium, labeled as medium 1 in the figure. Non-uniformity is introduced in the form of a spherical region (with radius = 1 cm) which is located at the origin of the Cartesian coordinate system. The spherical region contains a different medium with different physical properties**

As can be seen in figure A3.1, the particle is approaching the spherical region from the bottom whereas its direction of propagation is along the z-axis.

In addition, let's assume that the sampled distance to the next collision in the infinite and uniform medium, i.e. medium 1, is 2 cm and that the particle is located 1 cm away from the bottom surface of the spherical region. As the two media, medium 1 and medium 2, have different physical properties, it becomes important to check/calculate the intersection of the path of the particle with the spherical region. It is perhaps easier to think of this by drawing a straight line (see the dashed line in figure A3.1) from the current position of the particle (extending in both directions) and checking as to whether or not the extensions of this line cross any interfaces in the problem geometry. In the following, these calculations are described in detail.

Normally, the particle's position coordinates are updated, based on the sampled distance to the next collision and the direction cosines, as follows:

$$\begin{aligned} x &= x_0 + u\lambda \\ y &= y_0 + v\lambda \\ z &= z_0 + w\lambda \end{aligned} \qquad \text{(A3.1)}$$

where x, y, z are the updated position coordinates, x_0, y_0, z_0 are the current position coordinates of the particle in the Cartesian coordinate system, u, v, w are the direction cosines of the particle and λ is the sampled path length to the next interaction site.

Also needed is the quadratic equation of a sphere in order to calculate the intersection of the particle's path with the spherical region defining a different medium. Since the center of the sphere is located on the origin of the Cartesian coordinate system, this can be given as:

$$r^2 = x^2 + y^2 + z^2 \tag{A3.2}$$

The calculation proceeds by inserting equation (A3.1) into equation (A3.2):

$$\begin{aligned} r^2 &= (x_0 + u\lambda)^2 + (y_0 + v\lambda)^2 + (z_0 + w\lambda)^2 \\ r^2 &= x_0^2 + 2x_0u\lambda + u^2\lambda^2 + y_0^2 + 2y_0v\lambda + v^2\lambda^2 + z_0^2 + 2z_0w\lambda + w^2\lambda^2 \\ \lambda^2(u^2 + v^2 + w^2) &+ 2\lambda(ux_0 + vy_0 + wz_0) + x_0^2 + y_0^2 + z_0^2 - r^2 = 0 \end{aligned} \tag{A3.3}$$

Furthermore, for ease of notation, the following are introduced:

$$\lambda^2 + 2\lambda\vec{p}\bullet\vec{\Omega} + \rho^2 - r^2 = 0 \tag{A3.4}$$

where $u^2 + v^2 + w^2 = 1$, $\vec{p}\bullet\vec{\Omega} = ux_0 + vy_0 + wz_0$ and $\rho^2 = x_0^2 + y_0^2 + z_0^2$.

Equation (A3.4) is a quadratic expression and its roots are found by examining its discriminant as follows:

$$\lambda_{1,2} = \frac{-2(\vec{p}\bullet\vec{\Omega}) \pm \sqrt{4(\vec{p}\bullet\vec{\Omega})^2 - 4(\rho^2 - r^2)}}{2} = -(\vec{p}\bullet\vec{\Omega}) \pm \sqrt{(\vec{p}\bullet\vec{\Omega})^2 - (\rho^2 - r^2)} \tag{A3.5}$$

The two solutions of equation (A3.4) given in equation (A3.5) have the following physical meanings:

- If both solutions are positive, it can be concluded that the particle is located outside the spherical region and the positive extension of its path will cross both sides of the sphere, i.e. the particle is approaching the spherical region. In this case, the minimum of the two positive solutions will be taken as the distance to the nearest interface.
- If both solutions are negative, it can be concluded that the particle is located outside the spherical region and the negative extension of its path will cross both sides of the sphere, i.e. the particle propagating away from the spherical region. As the spherical region is not on the particle's path, it need not be taken into account while sampling the distance to the next collision site.
- If equation (A3.5) has two solutions, one of which is negative and the other is positive, it can be concluded that the material is within the spherical region. Only the positive solution needs to be taken into account as this will be the distance to the exit point.

Also, the term in the square root in equation (A3.5) might be negative. The physical meaning of this is that neither the positive nor the negative extensions of the particle's path will cross

the spherical region, and that it need not be taken into account during sampling of the distance to the next collision site.

In this particular example given here (see figure A3.1), upon substituting the numerical values of all parameters into equation (A3.5), it is found that the relevant quadratic equation has two positive solutions, $\lambda_1 = 3$ cm and $\lambda_2 = 1$ cm. Obviously, the minimum of the two solutions, i.e. λ_2, is the distance to the nearest interface the particle will encounter. The particle would then need to be first transported to the nearest interface (the interface between medium 1 and medium 2) as this distance is smaller than the sampled distance to the next interaction site in medium 1. Then a new path length to the collision site would have to be sampled from the exponential distribution using the physical properties of the new medium, i.e. medium 2.

APPENDIX 4: Example GMMC input file

```
0.718              ! The inner cathode radius (cm)
0.75               ! The outer cathode radius (cm)
0.05               ! Radius of the anode wire (cm)
3.616              ! Length of the anode wire (cm)
0.0006             ! Thickness of the inner cathode coating (cm)
3.9                ! The inner detector length (cm)
0.132              ! Radius of the anode tip bead (cm)
0.453              ! Distance from the inner front wall to the anode tip bead (cm)
0.118              ! Thickness of the back wall (cm)
0.0595             ! Initial photon energy (MeV)
0.0 0.0 -4.95      ! Position coordinated (x, y, z)
0 0 1              ! Initial direction (u, v, w)
1                  ! No. of insulating disks
-1.206             ! Position of the 1st disk
0.001              ! Thickness of the 1st disk
21                 ! No. of elements in the cathode material
26 0.70184         ! Element atomic number and weight fraction
24 0.2847          !
13 0.0047          !
25 0.0037          !
28 0.0018          !
23 0.0008          !
42 0.0004          !
06 0.00035         !
07 0.0003          !
29 0.0003          !
27 0.0003          !
15 0.00022         !
74 0.0002          !
12 0.00018         !
48 0.00005         !
93 0.00005         !
40 0.00005         !
50 0.00002         !
22 0.00002         !
16 0.00001         !
05 0.00001         !
7.55               ! Density of the cathode material (g cm^-3)
5                  ! No. of elements in the anode material
26 0.694           ! Element atomic number and weight fraction
24 0.284           !
14 0.014           !
25 0.005           !
28 0.003           !
7.42               ! Density of the anode material (g cm^-3)
7                  ! No. of elements in the anode tip bead and back wall material
14 0.5605          ! Element atomic number and weight fraction
```

```
82 0.2978       !
11 0.077        !
19 0.045        !
13 0.014        !
51 0.0035       !
25 0.002        !
2.47            ! Density of the anode material (g cm^-3)
3               ! No. of elements in the fill gas material
10 0.99403      ! Element atomic number and weight fraction
18 0.001        !
35 0.00498      !
0.0001          ! Density of the fill gas material (g cm^-3)
1               ! No. of elements in the cathode coating material
24 1            ! Element atomic number and weight fraction
7.19            ! Density of the cathode coating material (g cm^-3)
2               ! No. of elements in the insulating disk material
72 0.848        ! Element atomic number and weight fraction
08 0.152        !
9.68            ! Density of the insulating disk material (g cm^-3)
25000           ! No. of histories to be simulated
1 2             ! Initial seeds for the random number generator
0.001           ! Simulation cut-off energy (MeV)
```